Reconfigurable Power Combiner and Miniature Filter

by

Yamuna Jayan

A thesis
presented to the University of Waterloo
in fulfillment of the
thesis requirement for the degree of
Master of Applied Science
in
Electrical and Computer Engineering

Waterloo, Ontario, Canada, 2020

Declaration

I hereby declare that I am the sole author of this thesis. This is a true copy of the thesis, including any required final revisions, as accepted by my examiners.

I understand that my thesis may be made electronically available to the public.

Abstract

Microwave communication systems have undergone tremendous changes in the past two decades. There is an ever growing demand for devices with higher performance, lower cost and smaller size. Hence, more focus is given to improving the operational efficiency of individual devices. Microwave filters and power combiners are essential parts of such communication systems. This thesis presents a novel reconfigurable power combiner and a unique design for a miniature filter design, which can operate either as an ultra wide band (UWB) filter or a dual-band filter.

A Gysel power combiner(GPC) is used to combine input signals from two high power amplifiers. However, the performance of conventional GPC degrades in the case of an imbalance between inputs. With the failure of one of the power amplifiers, only half the power of the other amplifier is delivered to the output port. The other half is dissipated in the load resistors. To circumvent this issue a reconfigurable Gysel combiner is proposed. The reconfigurable Gysel combiner operates efficiently in the normal operational mode. In the case of a failure of one of the amplifiers, it delivers the full power of the other amplifier to the output port. The new design for the reconfigurable Gysel combiner incorporates six SPST switches and a stub matching network.

A filter is a two-port device used for frequency selectivity in microwave communication. Among which the UWB filters have a wide pass-band (>20%) and support high data rates, while the dual-band filters are used in multi-band communications. This thesis introduces a unique method to design miniature UWB and dual-band filters. A capacitively coupled distributed microstrip filter with N resonators is integrated with lumped capacitors to effectively produce 2N+1 resonators. This filter can be transformed into a UWB or a Dual-band filter depending on the value of the lumped capacitor.

Prototype units for the reconfigurable Gysel combiners, UWB filter and dual-band filter have been developed, fabricated and tested.

Acknowledgements

I wish to express my sincere appreciation to my Supervisor, Dr.Raafat Mansour, for the excellent guidance and encouragement he provided throughout my graduate studies. He is a distinguished Engineer and an outstanding teacher who motivated me to pursue my goals and helped me in achieving it. He supported me in hard times and helped me in adapting to Canada and the University of Waterloo. Without Dr.Mansour's supervision, this thesis wouldn't be possible.

I wish to extend special gratitude to Dr.Mohamed Fahmi for providing me with the idea for this thesis and his assistance in completing it. He helped me in understanding the new concepts and guided me whenever I hit a roadblock. I wish to thank Dr.Li Zhu, who was instrumental in my decision to pursue higher studies and joining UW. I would also like to acknowledge Dr.John Long, Dr. C.Selvakumar, Dr.Omar Ramahi, whose courses broadened my knowledge in different fields of electrical engineering.

I want to thank all my dear friends from UW, who helped me in various ways in completing this thesis, especially Rithwik Kodamana, who assisted me with organizing and editing. I thank Navjot Khaira, my office mate and dear friend, for supporting and motivating me for the past two years. I am grateful for the technical assistance provided by my CIRFE lab mates Junwen Jiang(Frank), Tejinder Singh and Farzad Yazdani. I am thankful to Shaeera Shuvra for helping me in better understanding the RFIC Engineering course. I am also extending my gratitude to all others in case if I forgot to mention their names.

Last but not least, my friends and family back home in India and in Canada, I am forever grateful for your presence in my life. To my parents N.Hema and K.N.Jayan, I am indebted to you for supporting me in all my endeavours and being my backbone. I will not be able to express my gratitude and respect for them in mere words. I am obligated to my grandmother Swarnakumari for being light of my life and inspiring me to be a strong woman. Finally, my siblings Vijay and Anjana for making my life special and my cousins Jyothi, Aswathi and Rajath for always being there for me.

Dedication

This thesis is dedicated to my beloved parents, grandmother and siblings for the encouragement and support they provided me all my life.

Table of Contents

List of Tables

List of Figures

Abbreviations

ASM Aggressive Space Mapping 13

GPC Gysel Power Combiner 1, 2

UWB Ultra Wide Band 1

Chapter 1

Introduction

1.1 Motivation

Microwave frequency ranging from 1GHz to 300GHz are extensively used for satellite communications, cellular communications, navigation and many other applications. The planar filters and power combiners are key components in a wide range of microwave circuits. The important design considerations of such microwave components are cost, weight, footprint and suitability to mass fabrication. This work presents unique designs of a reconfigurable Gysel Power Combiner (GPC) and a miniature Ultra Wide Band (UWB) Filter.

Gysel combiners are used to combine the power from two high power amplifiers into one output port. However, if one of the amplifier fails, only one half of the power of the second amplifier is delivered to the output. The remaining half is dissipated at the loads. This work introduces a novel reconfigurable Gysel that circumvents this issue. In case of failure at one amplifier port, the reconfigurable Gysel combiner allows the power from the other amplifier to be fully delivered to the output port.

Microwave filters are indispensable components in modern wireless communication systems. There have always been demands to reduce the size of filters. This thesis outlines a unique method to design miniature UWB, and dual-band filters. The proposed concept shows that by adding lumped capacitors to a capacitively coupled microstrip filter, the circuit can be transformed into either a UWB or a Dual-band filter.

1.2 Objective

The three main objectives for doing this work is listed below :

- Understand the background and working of conventional GPC.
- Development of a Reconfigurable Gysel Power Combiner that can operate efficiently if one of the amplifiers fails.
- Development of miniature wideband and dual-band filters.

1.3 Thesis Outline

The thesis is divided into five chapters first being Introduction. Chapter 2 presents a literature review, giving an overview of past work done by various researchers in Gysel power divider and the future trends. Chapter 3 presents the reconfigurable Gysel Power Combiner incorporated with switches and matching network. Chapter 4 presents results of a miniature wideband and dual-band filter. The last Chapter 5 is dedicated for conclusions, research findings and proposed future design improvements.

Chapter 2

Literature Review

Power dividers or power combiners are one of the fundamental building blocks of modern communication systems. They split or combine the power from the input ports to the output ports. The Gysel Power Divider introduced in 1975, is one of the most sought after power dividers. But the constant improvement in the modern communication fields calls for more sophisticated devices. This chapter discusses the modern state-of-the-art Gysel Power Dividers as well as the current and the future trends in the field.

Conventional Power Divider

The words power divider and power combiner are usually interchangeable. The same device can be used for both applications by merely swapping input and output ports. A simple T-junction is the most basic power divider. For all its simplicity a lossless T-junction cannot be matched at all ports and suffers from poor isolation. Hence researchers have come up with new techniques to achieve lossless condition and matched ports simultaneously.

A three-port Wilkinson power divider have the desirable properties such as matched ports, lossless power division and good isolation[5]. It was first introduced in 1960, and is one among the most commonly used power dividers. It is used in high power applications to combine solid-state transistor amplifier outputs or to split input signal to antenna array. But the major drawback associated with Wilkinson power divider is its dependence on internal resistor for good isolation. The inherent resistor in Wilkinson power divider is a lossy component and it is difficult to realize. It limits the power handling capability in high power applications[6].

However, when Ulrich H Gysel presented the N way Gysel Power Divider in 1975, it became an alternative to the traditional Wilkinson power divider[7]. The external isolation load resistors are the main advantage of the Gysel power divider. The grounded load resistor provides path for heat dissipation and does not limit the power handling capacity. Hence the only limiting factor of Gysel is the breakdown voltage of the transmission lines. Hence for the same frequency of operation Gysel is clearly superior to Wilkinson based on power handling capacity, geometry and easy realization.

A conventional Gysel Power Divider is represented in Figure 2.1b, it consists of five ports with two terminated at 50Ω load resistor. All transmission lines are of electrical length 90° at the center frequency, except the one connecting load resistors. U.H.Gysel did not provide any closed-form equations for calculating the impedance of the transmission line, so it is found using CAD software optimization. The power divider presented below splits the power equally between port 2 and port3. The outputs are in-phase and the impedance of branch line (Z_3) connecting load resistors controls the bandwidth of the device.

But the GPD occupies a larger surface area and it has limited isolation bandwidth. Therefore WPD took precedence over GPD in the initial years. Lately researchers have put a lot of focus in improving the performance of Gysel power divider. The following sections discusses the developments in the field.

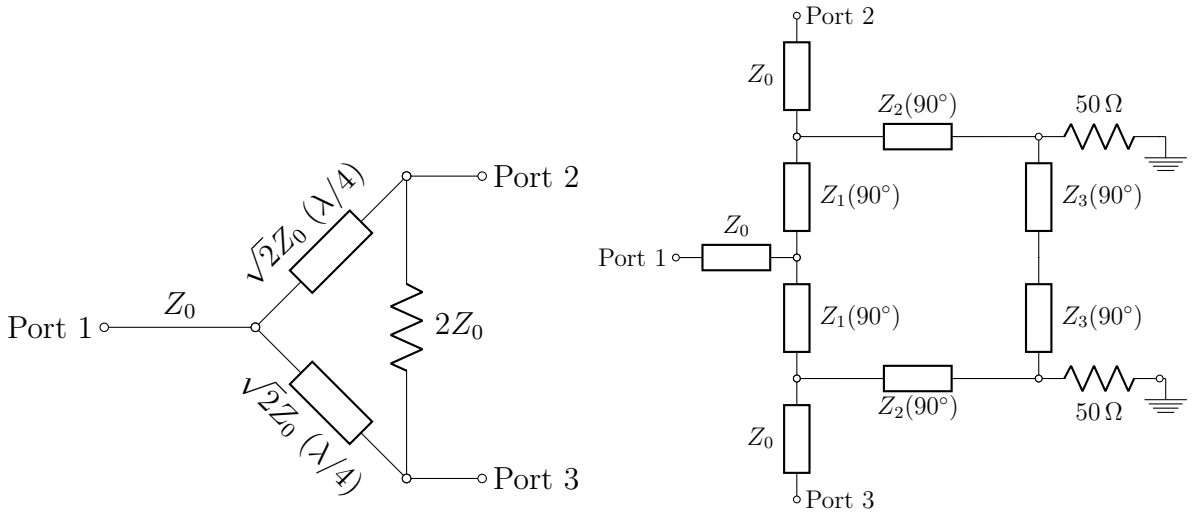

(a) Wilkinson Power Divider

(b) Gysel Power Divider

Figure 2.1: A simple layout of the two popular power dividers

Unequal Power Division

Most of the conventional power dividers splits the power equally between the output ports. But in many cases, power dividers are used as feed to array antennas which require unequal power division [8]. Traditionally achieving unequal power division needs complex mechanisms and impedance matching techniques. One of the widely used methods to achieve this is by un-even impedance method [9],[3]. It relies on the theory that more power is transmitted through smaller impedance. Hence the required power ratio can be obtained by controlling the line impedance. The downside to this approach is the fabrication problems associated with narrow lines widths. Another approach is to design patch-type Gysel[10] which eliminates the need of narrow line widths. But then the geometry and design become too complicated.

One of the advantages of Gysel combiners is that the electrical length of transmission lines does not affect the input impedance [2]. Reference [2] reported the possibility of achieving unequal power division by varying the electrical lengths without changing the impedance. The recorded operating bandwidth of the device is less than 10%, which is a major shortcoming. This theory is improved in [11] to achieve anti-phase and unequal power division by adding an 180° transmission line between input and output port.

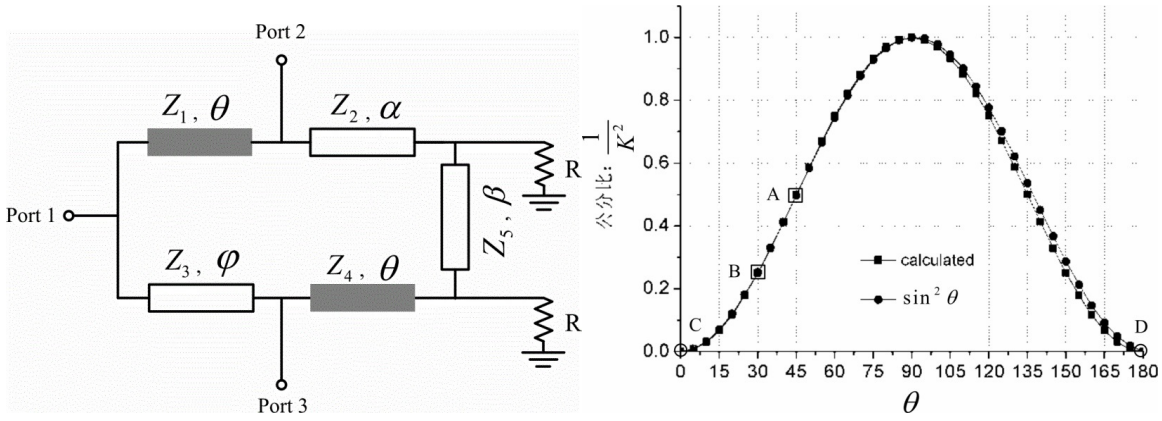

(a) Circuit (b) Power ratio Vs θ plot

Figure 2.2: The circuit for unequal power division described in [2] and b) the plot showing relationship between power ratio and electrical length θ

Increasing the Operating Bandwidth

A high isolation bandwidth reduces the possibility of positive feedback, diminish out-of band oscillations and decrease the spurious coupling between the input ports. But the main drawback of a conventional Gysel power divider is the narrow isolation bandwidth, typically less than 30%[10]. Researchers have come up with many interesting solutions to this problem.

A sequential matching technique suggested in [12] increases the bandwidth to 44% by changing the electrical length. A multi-stage-GPD approach presented in [13] increased the 20dB isolation bandwidth to 44% at the cost of increased area. In [14], a multistage Gysel power divider with bent transmission line and chip resistors reported to increase the isolation bandwidth to 63%. But multi-stage GPD increases the total area of the device which is undesirable.

The compact patch-type GPD addressed in [10] increases the isolation bandwidth by 30% with reduced area. But the design of the patch itself is very troublesome and it has a complex geometry. Another method suggests that by adding an L type matching network to the input of single-stage Gysel increase the isolation bandwidth to about 60%[3]. It also supports unequal power division using un-even impedance technique.

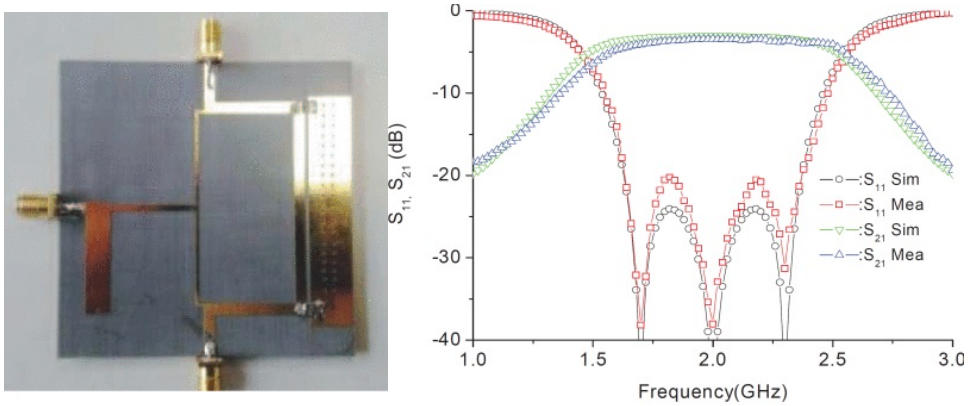

(a) Layout (b) Response

Figure 2.3: The layout of GPD with L-type matching network from [3] and b) the experimental results obtained

Modified Gysel Power Divider

The Gysel power divider and Wilkinson power divider have many advantages and disadvantages. But combining the two circuits together produce a better performance than what it does individually. In the modified power divider, the central resistor R1 from Wilkinson power divider (as shown in Figure 2.4) increases the isolation bandwidth. An earlier work [4] demonstrated this theory and the results show that isolation bandwidth has increased to 63%. And it has higher heat sinking capability compared to traditional WPD. But the disadvantage of the circuit is the presence of three resistors, one from Wilkinson and two from Gysel. A modified circuit presented in [15] improves this to an extent by reducing the number of external resistors to two. It also has a better bandwidth performance compared to previous work.

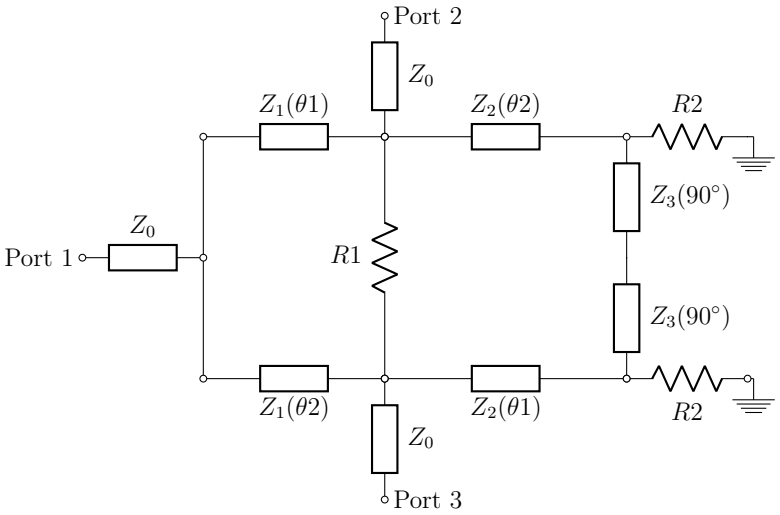

Figure 2.4: A schematic of the modified Gysel power divider suggested in[4]

Multi-band Power Divider

The present day communication network works at multiple frequency standards and hence there is a huge demand for device which cover multiple bands. A conventional Gysel with a short circuit stub in the input junction and an open circuit stub in the middle of the branch line between isolation resistors(Figure 2.5b) act as a dual-band power divider[16]. In

that case, all transmission lines have same electrical length θ_0, and dual-band performance depends on impedance values and θ_0. The paper also provides a closed-form equations for the circuit. The device have a reasonable isolation and return loss but suffers from poor fractional bandwidth. This theory is modified in [9], but they used coupled transmission lines. It eliminates the short circuit stub, reduces the overall size of the device and has better fractional bandwidth.

But most dual-band power divider suffers from lower isolation bandwidths. Another paper [17] proposed a new idea by improving the modified Gysel with an open stub as shown in Figure 2.5a. All transmission lines have the same electrical length θ_0, and conductance value g determines the frequency ratio. According to the paper higher value of g contributes lower bandwidth and high power handling capacity. The work reported a dual-band Gysel(1GHz and 2GHz) with 73% isolation bandwidth.

In a conventional GPD, the quarter-wave transmission line connecting the load resistor act as a phase inverter. Replacing it with dual band phase inverter results in dual-band operation. The Π shaped Composite Right/Left handed transmission line is used as dual-band inverter in [18]. The major advantage of CRLH is size reduction.

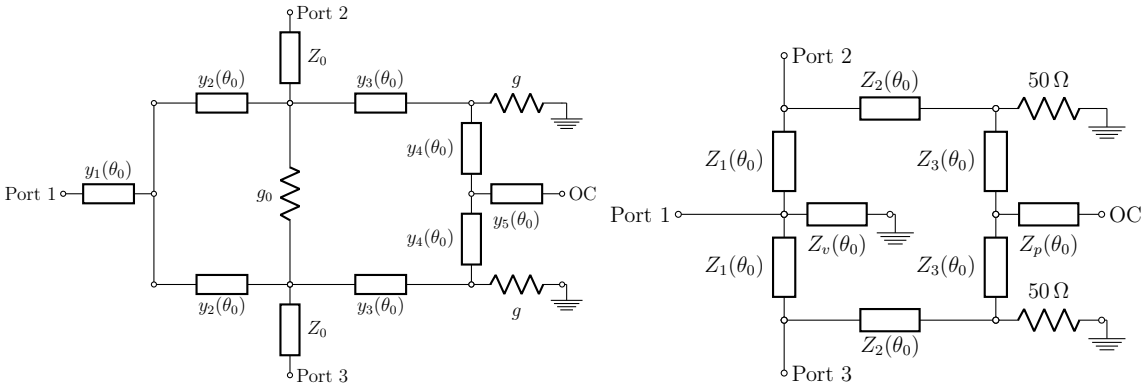

(a) Dual-band Modified GPD[17] (b) Dual-band GPD with stubs[16]

Figure 2.5: Two modified Gysel power divider circuits used to achieve dual-band operations

Researchers are also investigating tri-band power dividers. In [19], a multi-band phase inverter consist of trunk lines and a matching network replaces the traditional quarter-wave line inverter. Results shows a tri-band power divider operating at 1.93GHz, 2.47GHz and 3.07GHz with reasonable bandwidth and good isolation and return loss.

These days research has shifted to the design of dual-band structures with different power dividing ratios. The circuit in [16] is modified in [21] by adding transmission lines

Table 2.1: A review of previous works in multi-band power divider

Ref	Technology	f1/f2/f3 (GHz)	Return loss	Isolation	FBW	Power Ratio
[16]	Short& Open-end stub	1.0/2.0	>20dB	<20dB	6.5%,6.5%	1:1
[9]	Coupled-lines and open stub	1.0/2.0	>20dB	<16dB	7.5%,7.3%	1:1
[20]	Dual-band phase-inverter	1/2	>20dB	>25dB	12%,5.58%	1:1
[19]	open end stub	2.0/2.5/3.0	>19dB	>20dB	13%,14%,10%	2:1
[18]	CRLH TL	2.4/3.5	>20dB	<20dB	2.9%,8.6%	1:1

before Port 2 and Port3 to achieve unequal power division. It achieved the objective, but the power dividing ratio in the upper band differs from lower band. One of the recent papers [20] explains how to modify ordinary dual-band design by adding dual-band phase inverter between isolation resistors. Based on the paper electrical length and impedance values of transmission line controls the power dividing ratio. They designed dual-band Gysel for 1GHz and 2GHz with two power dividing ratios K = 1, K= $\sqrt{2}$ and reported fractional bandwidth of 10% and 5.5%.

Miniaturization of Gysel

Modern communication system demands devices with a smaller footprint. And the biggest disadvantage of GPD is its large size compared to the Wilkinson power divider. The easiest way to tackle this issue is by bending the transmission lines[17]. But bending the line can increase the interference and complicates the design. Researchers have come up with smarter solutions to this problem.

Eliminating the $\lambda/2$ line connecting the termination loads reduces the overall area to a larger extent. The coupled-line Gysel combiner reported in [22] implemented this technique. The circuit used is a combination of Gysel and Wilkinson with $\lambda/2$ line replaced by isolation resistor R_g. It reduced the area significantly, improved the operating bandwidth and supports the arbitrary power division. But the presence of R_g increases the power loss and limits power handling capacity. In [23], GPD is improved by using a pair of transmission line, a coupled line, a single resistor and eliminating $\lambda/2$ line. The circuit works good for

(a) Coupled Line GPD[23]

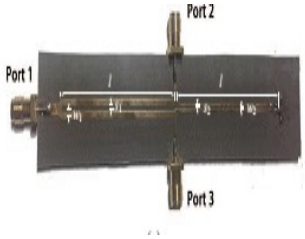

(b) Coupled Line GPD[22]

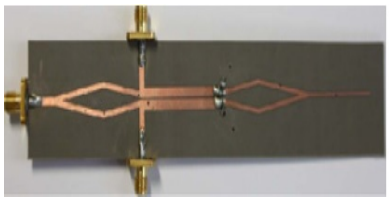

(c) Coupled Line GPD[9]

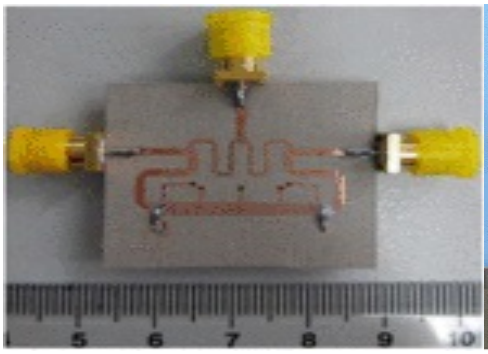

(d) GPD with CRLH Line [18]

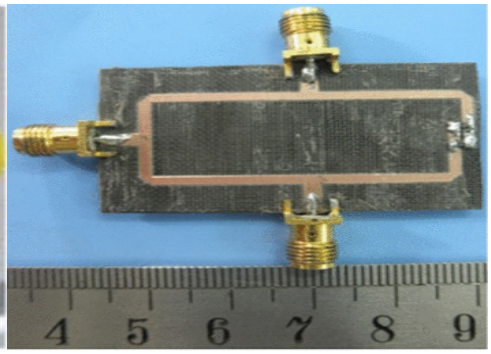

(e) GPD with phase inverter[24]

Figure 2.6: A sample of GPD layouts that successfully achieved miniaturization

unequal power division but equal power division requires an additional resistor. Coupled-line Gysel is further improved in [9] to support dual-band operation by adding an open circuit stub.

The composite Right/Left handed transmission line Gysel mentioned in [18] also rule-out the $\lambda/2$ transformer to reduce the size. The 180° phase inverter is replaced by a microstrip to slot-line combination in [24], and it shrunk the circumference to $1\lambda_0$.

Non-planar Gysel Power Divider

The future mmwave technology requires advanced devices which can work at high frequencies with low insertion loss, smaller size, high power handling capability and easy integration properties. Until the end of 2014, most of the effort was focused on the design of planar power dividers which are used for low-frequency applications. The metallic waveguide based power dividers have higher power handling capacity and can work at high frequencies. But it is usually bulky and difficult to integrate to planar circuits.

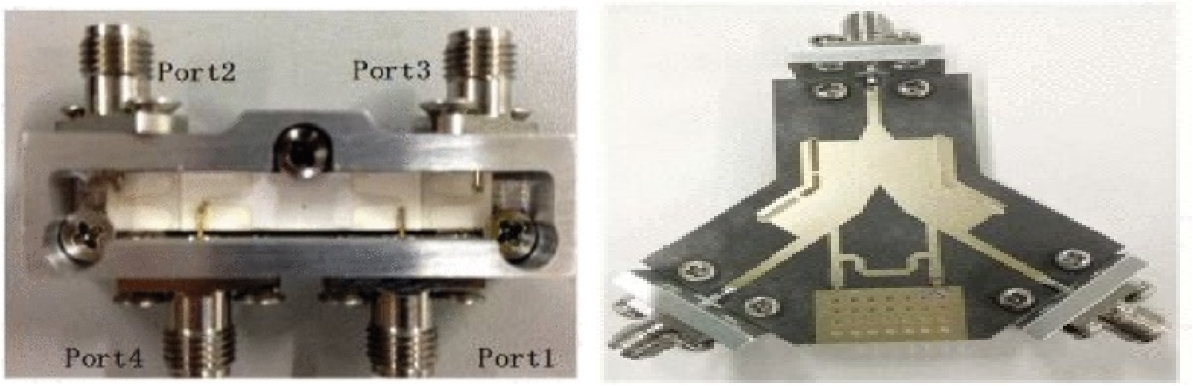

(a) SIW Gysel from[28] (b) HMSIW Gysel from[27]

Figure 2.7: Layouts of two non-planar Gysel power dividers using SIW and HMSIW techniques

The Substrate-Integrated-Waveguide proposed in 2001 [25], received wide interest in the last decade. The SIW have the advantages of both waveguide and microstrip. They are low loss, low cost, low profile devices having high power handling capacity compared to traditional microstrip circuits. It can be integrated easily into larger high density circuits and is projected to replace waveguide structures in mmwave circuits[26].

A planar Gysel Power Divider based on SIW technology is reported in 2015[27]. It works at 10GHz and has 5.5% fractional bandwidth and good isolation. But it occupies relatively larger area and is hard to integrate with other planar circuits. To overcome this problem a new size reduced multi-layer SIW Gysel power divider based on LTCC technology is proposed[28]. It reduced the overall area by 83% and has acceptable return loss and isolation at 18GHz.

A newer technology Half-Mode-Substrate-Integrated-Waveguide [29], overcomes the limitations of SIW and reduce the area by half. It may be better suited for mmwave applications than ordinary SIW devices. A HMSIW Gysel power divider designed for 7.5GHz[27] is reported to have good return loss and isolation. But the larger value of insertion loss is a huge concern.

Researchers are keen on solving the issues with SIW and HMSIW circuits. These technologies are predicted to dominate the future mmwave industry.

Summary

Gysel power dividers are used in microwave circuit for power division in high power applications. This chapter discussed the previous works done in GPD by various researchers and the progress achieved in the field. Initial works in GPD were mostly focused in achieving unequal power division, dual-band operation, miniaturization and improving the operational bandwidth. Lately the research is moving towards the non-planar GPD using SIW and HMSIW techniques. The GDP's are expected to play a prominent role in the upcoming microwave circuits.

Chapter 3

Reconfigurable Gysel Power Combiner

Gysel power combiners are used in modern communication systems to combine input signals from amplifiers in high power applications. In general, there is some inherent problem associated with coupler-based power combiners when dealing with the failure of one amplifier. If one amplifier fails and the input signal from that amplifier is lost, one half of the power of the second amplifier will be dissipated in the load resistors. This chapter introduces an approach to deal with this issue. If a fault is detected with one amplifier, the combiner is reconfigured so that the input power from the second amplifier is diverted fully to the output rather being split between the output and the loads. To achieve this objective, switches and a matching network are added to the Gysel combiner. Initial designs are carried out in ADS schematic software and final circuit is verified using Sonnet EM simulation. The Aggressive Space Mapping (ASM) was used to fine tune the design of the reconfigurable Gysel combiner. This chapter also explains the steps followed in creating an ASM mapping between ADS schematic coarse model and Sonnet EM fine model.

3.1 Gysel Power Combiner

A basic Gysel power combiner is a five port device with two ports terminated at 50Ω resistors as shown in Figure 3.1. It combines the input signal from Port 2 and Port 3 constructively and delivers it to the output Port 1. The impedance values of Z_1, Z_2, Z_3 determine the power ratio and bandwidth of the combiner. The advantage of Gysel design

over the traditional Wilkinson power divider is the presence of external loads which helps to increase the power handling capability and thermal efficiency of the device. The following section describes the design of a simple Gysel power combiner.

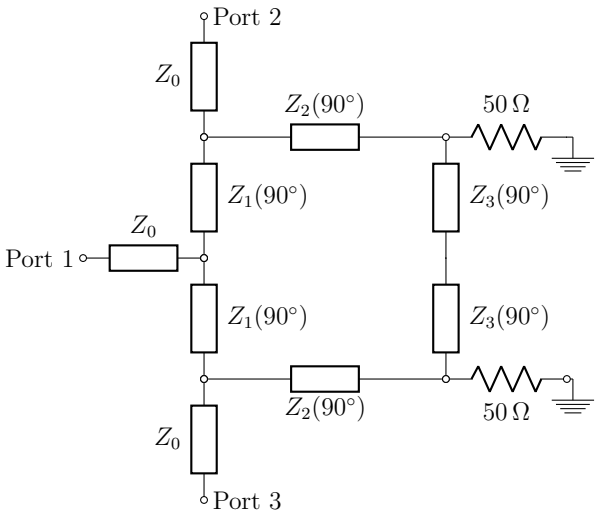

Figure 3.1: Schematic of a conventional Gysel power combiner

3.1.1 Ideal Gysel Power Combiner

An ideal GPC is designed to work at a center frequency of 2GHz using ideal circuit components in ADS. Figure 3.2 shows the ADS schematic used for the design. For this design, the transmission lines with electrical length $\lambda/4$ and impedance Z_1=70.7Ω, Z_2=50Ω, Z_3=35.35Ω are used. The ADS results obtained from analysis shows a power combiner at 2 GHz with a bandwidth of 400MHz as shown in Figure 3.2.

3.1.2 Power Failure at One Port

In a normal scenario, no power is dissipated in the load terminals. If the input from port 3 is lost completely then only half of the signal from Port 2 is transferred to Port 1, other half gets dissipated between the loads. The failure event can be simulated as an open circuit, short circuit as well as a complex impedance load. Figure 3.3a and 3.3c show the simulation results when port 3 is terminated by open circuit and short circuit respectively.

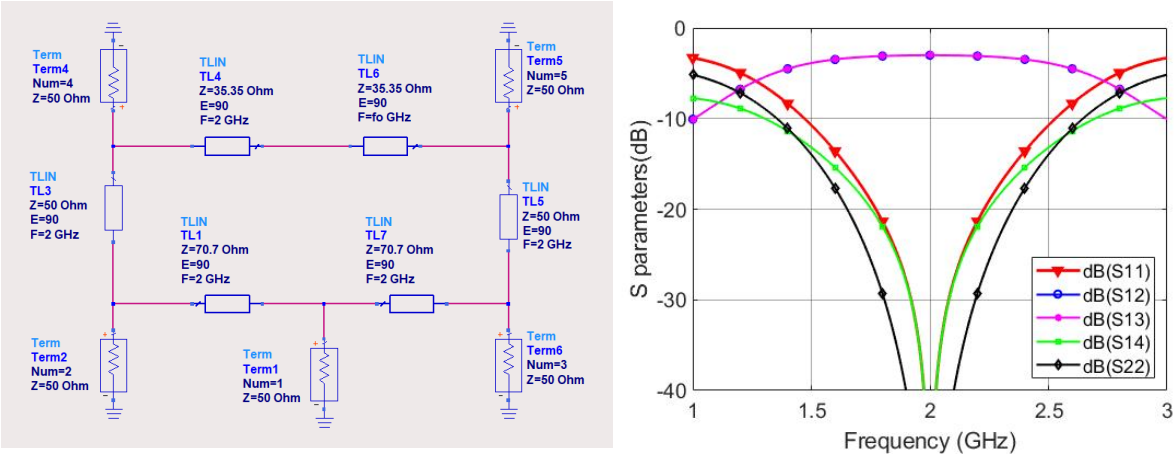

Figure 3.2: Ideal Gysel power combiner ADS schematic and results

The results show that only 3dB of the input power from port 2 is transferred to port1 and other half is shared by loads at ports 4&5.

This work proposes a Gysel combiner circuit integrated with switches and a matching network as shown in Figure 3.3e. We use 6 switches, one switch is used to impose short circuit failure at one port and the other five switches are used to reconfigure the power combiner so that the power from the other port is delivered to the output. A switched matching stub is added to Port 1, to improve the matching at the port 1 when the circuit is reconfigured. In normal operational conditions all switches are in the OFF state and the circuit delivers the input power from ports 2 and 3 to the output port 1.

When a failure is detected for example at port 3 (the switch S3 is located at this port is turned ON to impose the short circuit condition), the switches S1, S3, S4 and S5 are activated to route the input power from port 2 to the output port 1. Figure 3.3f shows the response obtained. The power from port 2 is delivered to the output port (port 1). Because of circuit symmetry, a short circuit failure at port 2, the combiner can be reconfigured such the power from port 3 is delivered to port 1. Table 3.1 summarizes the switches states in case of normal operation and failure at port 2 and port 3.

The matching network dimensions of the reconfigurable Gysel combiner after optimization are dX =56.75°, dL = 44.64°, Zstub = 72.18Ω. The insertion loss of the new circuit has been reduced significantly compared to the failure state outputs, but its operational bandwidth is almost half of the normal state response.

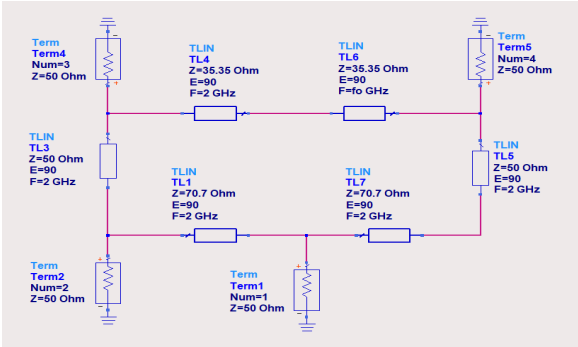

(a) Open Circuit

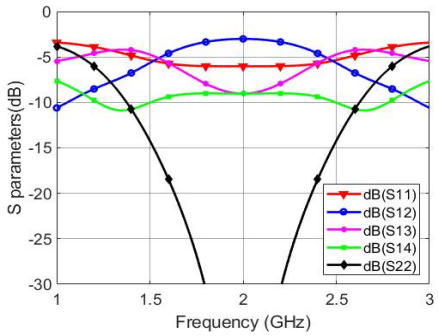

(b) Response

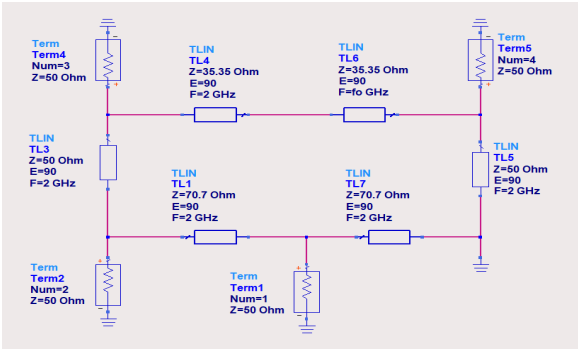

(c) Short Circuit

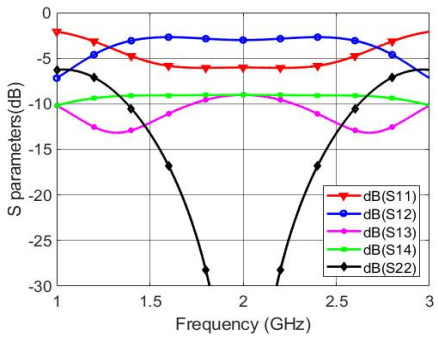

(d) Response

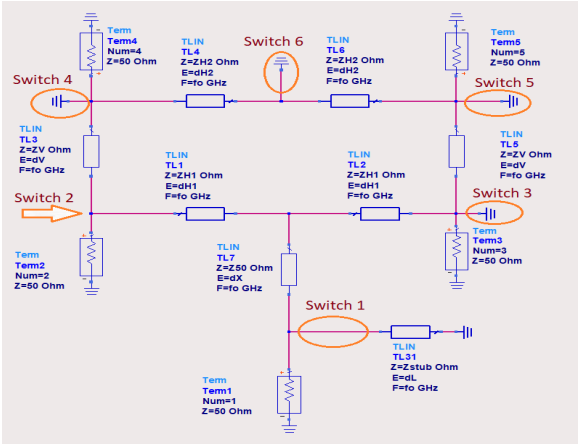

(e) With Switches

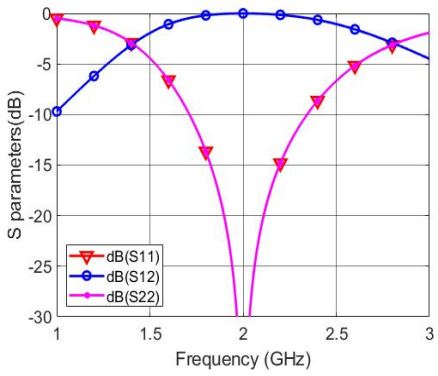

(f) Response

Figure 3.3: ADS schematic layout and results of ideal Gysel power combiner with faulty condition at port 3 and the reconfigurable circuit with switches

Table 3.1: Switches states in normal operation and in case of failure at ports 2 and port 3

State	S1	S2	S3	S4	S5	S64
Normal	OFF	OFF	OFF	OFF	OFF	OFF
Failure at port 2	ON	ON	OFF	ON	ON	ON
Failure at port 3	ON	OFF	ON	ON	ON	ON

3.2 Implementation of GPC in Microstrip

After identifying the ideal GPC circuit parameters, the next step is to trace it in microstrip. A microstrip substrate with height of 20 mils, dielectric constant 10 and a copper thickness of 35µm is chosen for this purpose. An equivalent circuit for the switch is used for the design as shown in Figure 3.4. The switch acts as a 0.05pF capacitor in the OFF state and 4Ω resistor in the ON state.

Figure 3.5 shows the ADS schematic circuit used for the initial microstrip design. The ideal circuit parameters need to be optimized to work for both the normal operation state and faulty state simultaneously. The final dimensions after optimization are provided in the Table 3.2 and the final response is shown in Figure 3.6. The microstrip transmission line lengths are shorter than the ideal 90° and impedances are also slightly different. These changes are made to meet the simultaneous working requirements of normal and faulty conditions of the combiner. The device works at 2GHz with a minimum of 400MHz bandwidth under normal condition and 200MHz bandwidth during faulty condition. It also has a good isolation (>20dB) between the input ports during both states.

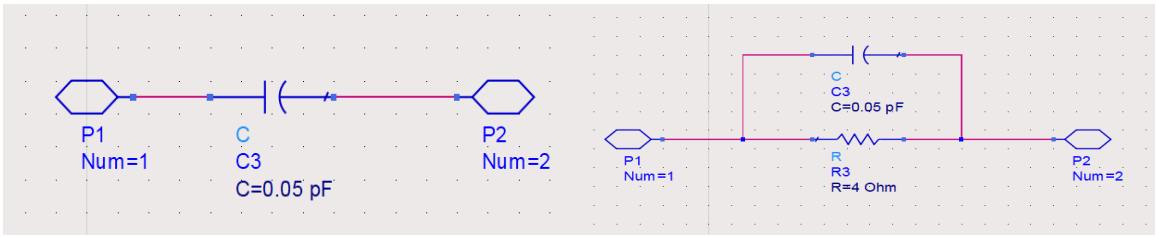

(a) OFF state (b) ON state

Figure 3.4: RF-MEMS switch equivalent circuit for OFF condition and ON condition

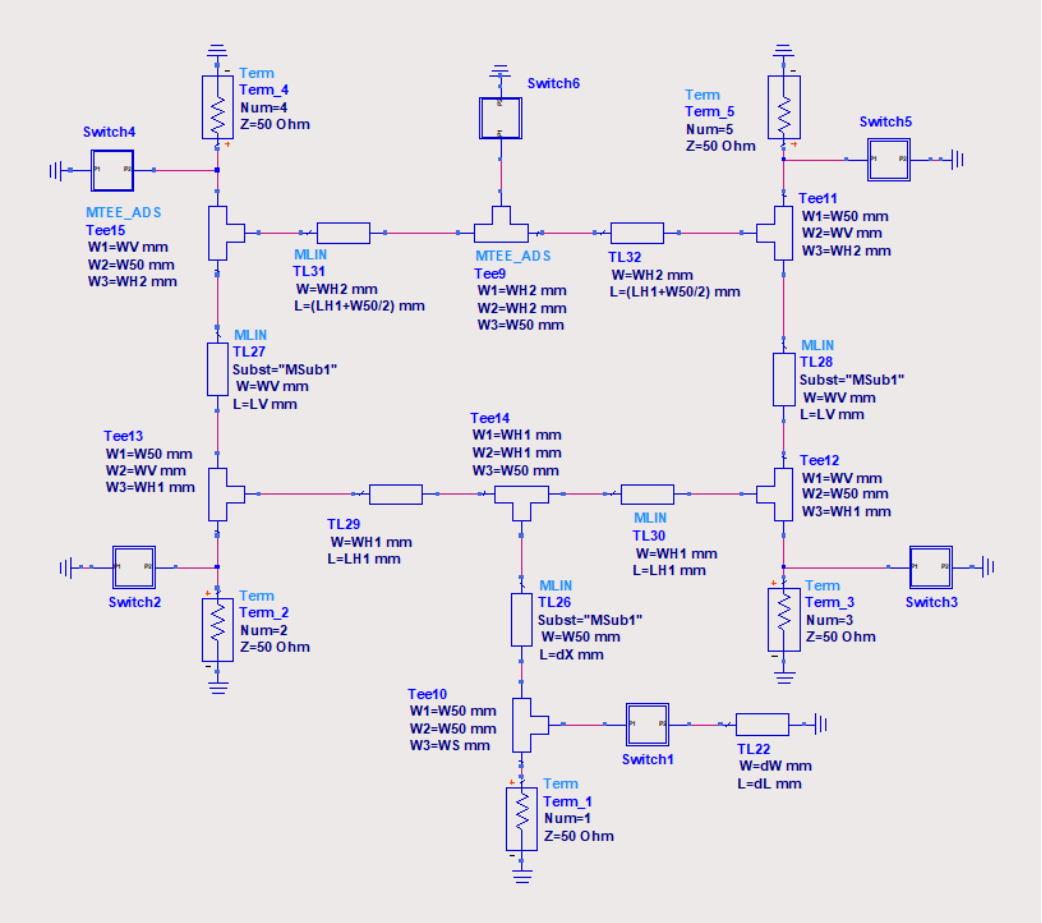

Figure 3.5: ADS schematic layout of microstrip Gysel power combiner with switches

3.3 EM Design Procedure for the Gysel Combiner

EM simulators such as Sonnet and HFSS provide accurate results compared to the ADS circuit simulator, but they tend to be time consuming. Hence it is easier to perform initial designs in ADS and transfer it to Sonnet in the final step. In most cases the ADS simulation results and Sonnet EM results show significant variation, and vigorous optimization is required to get an accurate result in Sonnet.

The aggressive space mapping technique [1] is used to obtain mapping between a circuit coarse model and an EM fine model. The established mapping can be used to obtain an accurate EM response with optimization only done in ADS and no optimization with the

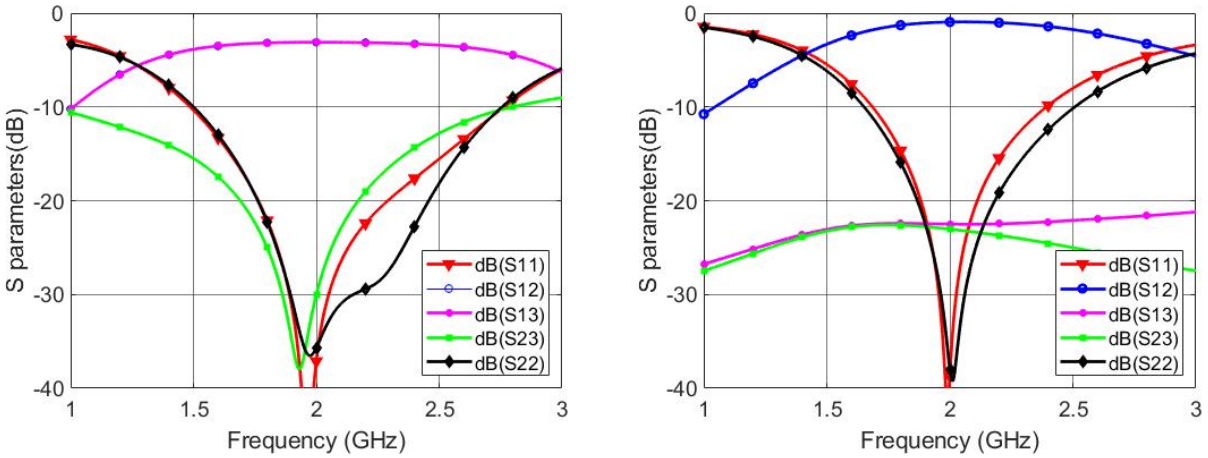

(a) Normal state (b) Switch ON state

Figure 3.6: Microstrip GPC response from ADS schematic simulation for normal state and failure at port 3

Table 3.2: Parameter values used in ADS schematic for microstrip GPC

Parameter	Value	Parameter	Value
W50(Width of Input Transmission Line)	0.45mm	WH1 (Width of Z_1 Transmission Line)	0.2027mm
WV (Width of Z_2 TL)	0.479mm	WH2 (Width of Z_3 TL)	1.755mm
LV (Length of Z_2 TL)	12.814mm	LH1 (Length of Z_1 TL)	13.575mm
dX (Distance to Stub)	11.11mm	DL (Length of Stub)	7.8mm
DW (width of Stub)	0.12mm	-	-

EM simulator. This section explains the steps followed in establishing a mapping between ADS coarse model and Sonnet fine model.

The first and the most important step is to achieve an accurate result in ADS circuit model which satisfy all design parameters. This ADS model is then used as the coarse model when applying the aggressive space mapping technique. The ideal circuit dimensions from ADS are used to build the layout for the Sonnet simulation. The Gysel power divider layout used for Sonnet simulation is shown in Figure 3.7 and the initial results obtained from Sonnet are illustrated in Figure 3.8a, 3.8b. As expected, the results of the ADS coarse model and the Sonnet fine model show significant differences. Hence Aggressive Space Mapping is performed to improve the Sonnet results.

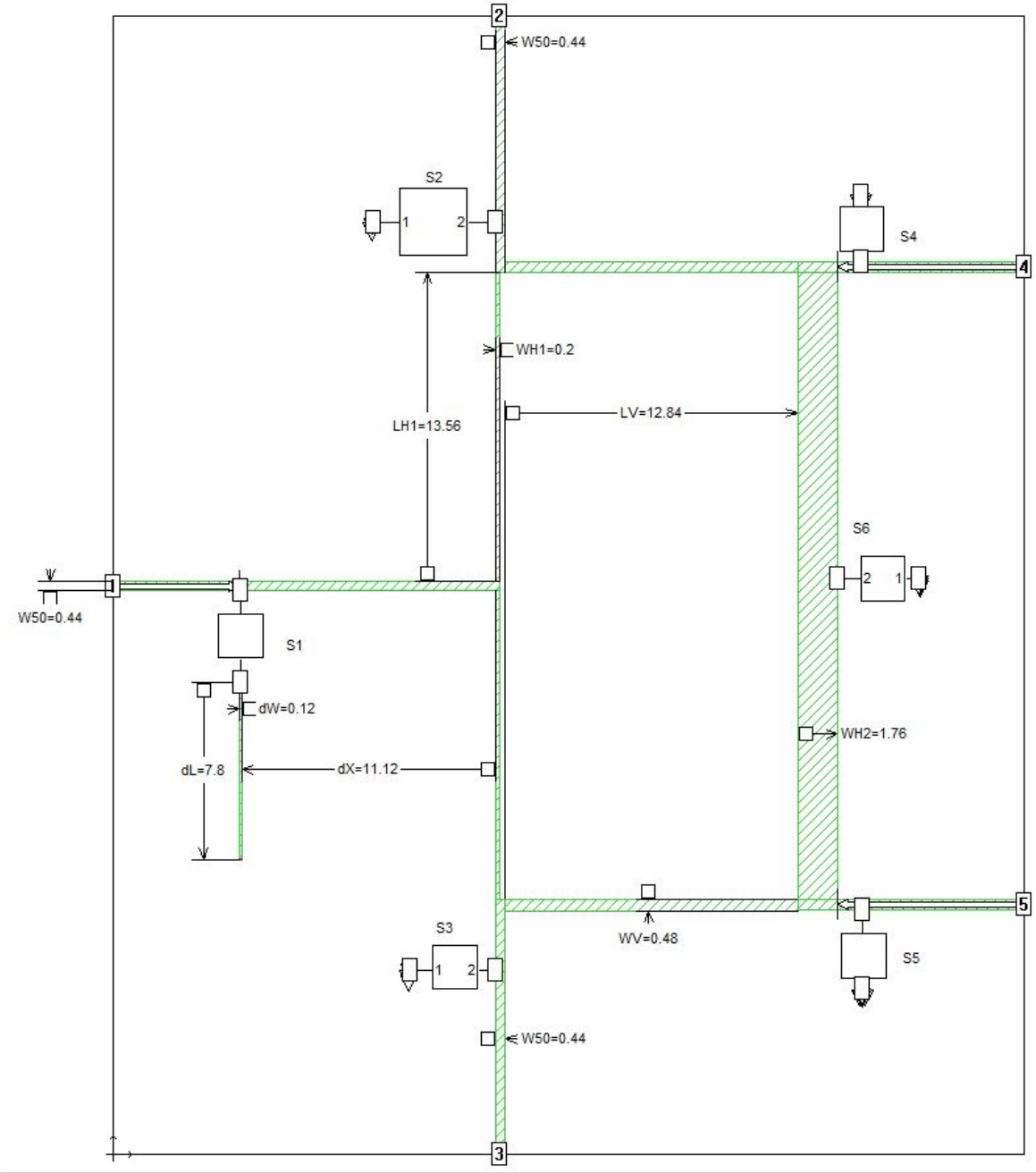

Figure 3.7: Sonnet layout for microstrip Gysel power combiner

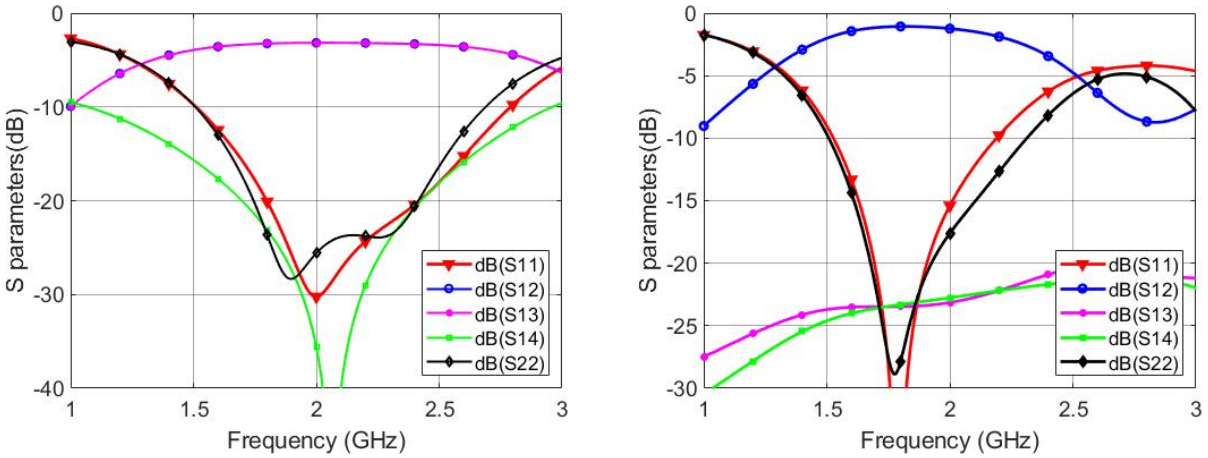

(a) Normal state (b) Switch ON state

Figure 3.8: Microstrip GPC response from Sonnet initial simulation for normal state and failure at port 3

In order to establish the mapping between fine model and coarse model[30], data samples are collected from Sonnet results(Switch ON and Switch OFF S11 plot) as shown in Figure 3.9. The ADS coarse model is optimized to replicate the exact sonnet EM results. The seven key parameters which affect the performance of the circuit are width of vertical line(WV), width of horizontal line(WH2), Length of vertical line(LV), Length of horizontal line(LH1), Length of offset line(d-off), Length of the stub(d-stub), distance to stub(dX). Hence these parameters are used as the optimization variables. The width of horizontal line(WH1) is kept as a constant due to its smaller dimension. A new set of parameter values are obtained after ADS optimization.

Iteration

- The initial set of optimization variables used in sonnet EM simulation is termed as Xf1 and the corresponding obtained set of values from ADS is termed as Xc1(Table 3.3).
- The equations mentioned in [1] are used and a new set of variable values for the fine model (Xf2) is obtained. The Sonnet response for the new set of parameter values

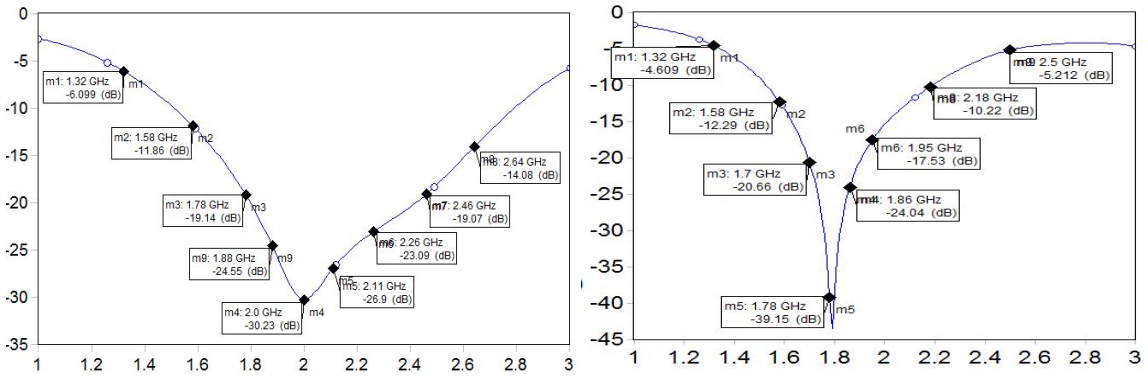

(a) Normal state (b) Switch ON state

Figure 3.9: Collecting samples from Sonnet initial EM response for space mapping

are shown in Figure 3.10c, 3.10d. It is evidently better than the initial result but still varies from the ideal circuit response.

- The data samples are again collected from the new response. From ADS optimization, a new set of coarse model values (XC2) is obtained.
- The equations from [1] are used again to find new Xf3 values. The results from Sonnet (Figures 3.10e, 3.10f) are closer to the ideal response for output return loss S_{11} and isolation S_{23}, but the input return loss shows significant variation. Hence the iterations are continued until a satisfactory result is obtained.

After four iterations the Sonnet EM fine model results(Figure 3.10g, 3.10h) resembles the ideal ADS coarse results. It is centered at 2GHz with 450MHz OFF-state and 200MHz ON-State return loss bandwidth. All the parameter values obtained from each iteration are tabulated in Table 3.3.

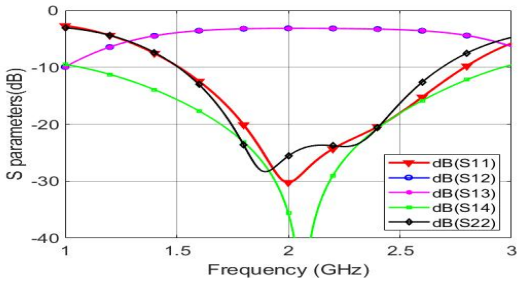

(a) Iteration 1 OFF-STATE

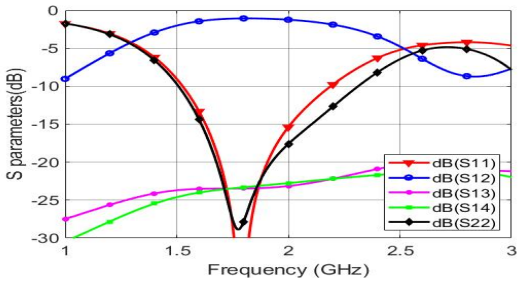

(b) Iteration 1 ON-STATE

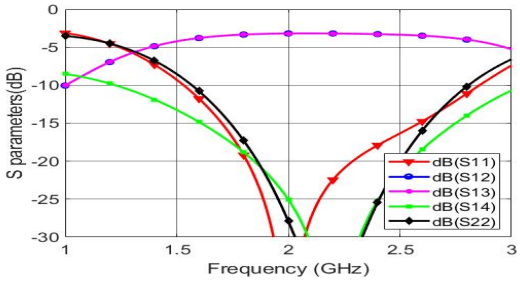

(c) Iteration 2 OFF-STATE

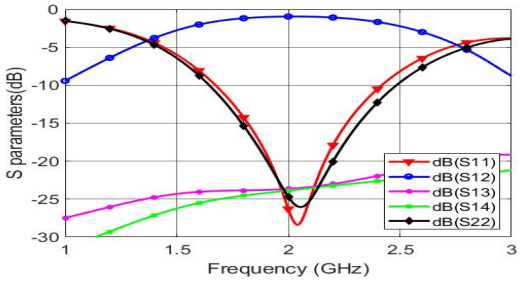

(d) Iteration 2 ON-STATE

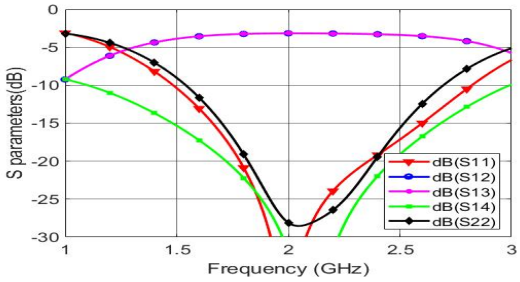

(e) Iteration 3 OFF-STATE

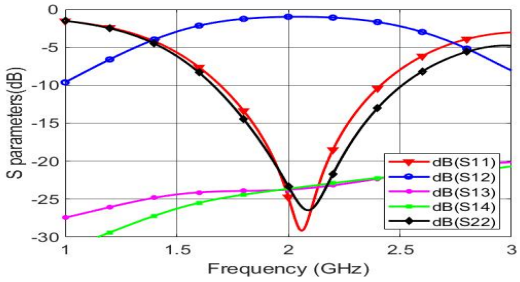

(f) Iteration 3 ON-STATE

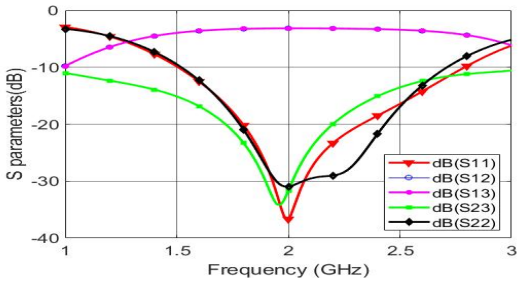

(g) Iteration 4 OFF-STATE

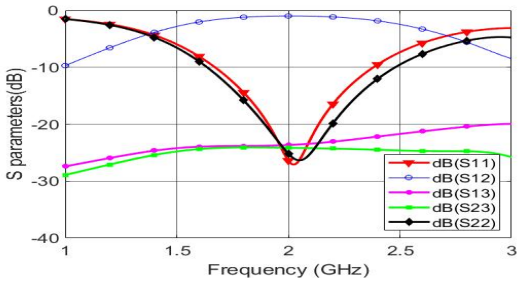

(h) Iteration 4 ON-STATE

Figure 3.10: Aggressive space mapping results after each iteration from Sonnet simulation

Table 3.3: Parameter values from ASM iterations

ASM		LH1(mm)	LV(mm)	WH2(mm)	WV(mm)	dL(mm)	dW(mm)	dX(mm)
Iteration 1	Xf1	13.575	12.816	1.754	0.4879	7.80	0.12	11.12
	Xc1	14.451	12.3986	2.1909	0.584	7.483	0.08	12.676
	f1	0.8756	-0.4174	0.4369	0.0961	-0.3170	-0.0400	1.5560
	h1	-0.8756	0.4174	-0.4369	-0.0961	0.3170	0.0400	-1.5560
Iteration 2	Xf2	12.6998	13.2334	1.3171	0.3918	8.1170	0.1600	9.5640
	Xc2	12.9732	12.885	1.4939	0.4547	8.0495	0.1179	11.7156
Iteration 3	Xf3	13.3322	13.1609	1.5902	0.4267	7.8550	0.1622	8.9386
	Xc3	13.5085	12.851	1.8	0.4608	7	0.0783	10.839
Iteration 4	Xf4	13.3502	13.1399	1.5460	0.4439	8.4227	0.1911	9.1620
	Xc4	-	-	-	-	-	-	-

3.4 Folded Transmission Line Gysel Power Combiner

The final Sonnet EM design obtained in the previous section requires six SPST switches and has an area of 40X40mm. By folding the Gysel combiner horizontally by WV line, reduces its size and makes it possible to use less number of switches. Hence, folding the transmission line reduces the total switch count from six to four and decreases the total area of the device. It should be noted that the circuit with only 4 switches requires the use of SPDT switches, with one of its states that allows the input to be connected simultaneously to the two output ports.

The length of WV line is reduced to 3.86mm closer to the switch dimension. Other parameters are adjusted slightly to compensate for the changes caused by folded line. The final Gysel combiner layout is shown in Figure 3.11a and Figure 3.11b and 3.11c shows the results. The input return loss bandwidth during OFF-state and ON-state are 465MHz and 195MHz respectively. The total area of the folded device is 24X40mm almost half of initial design shown in Figure 3.7.

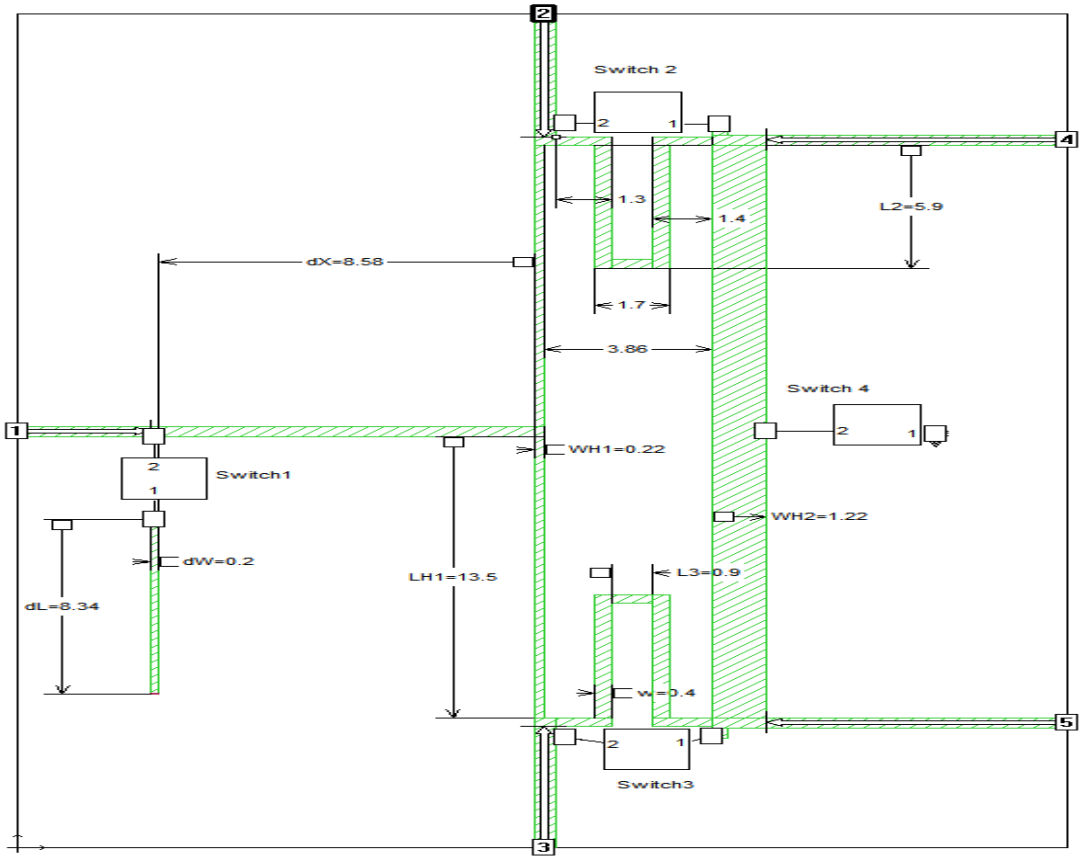

(a) Folded Gysel Combiner

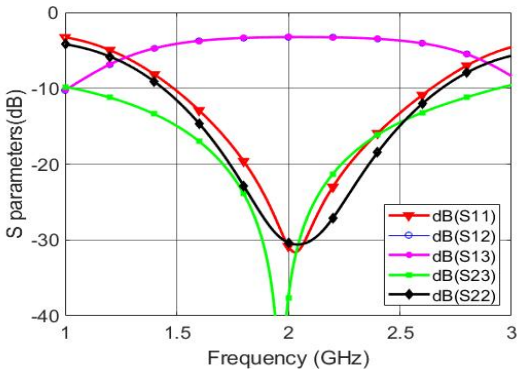

(b) Normal state

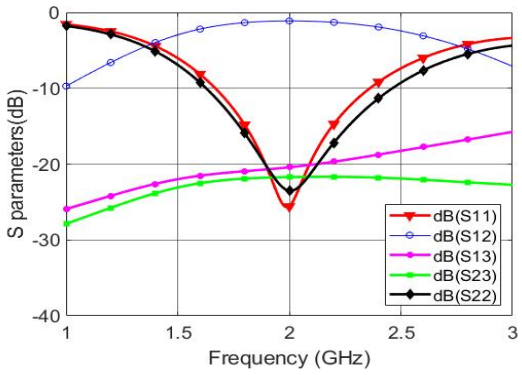

(c) Switch ON state

Figure 3.11: Sonnet layout for folded microstrip GPC and the EM response for normal and faulty states

3.5 Measured Results

Figure 3.12b shows the fabricated circuit layout, while Figure 3.12c, 3.12d shows the measured results for both the normal operation and the faculty operation. The experimental results for the faulty case were obtained using a circuit with a short circuit created by Via rather than by a switch to demonstrate the concept.

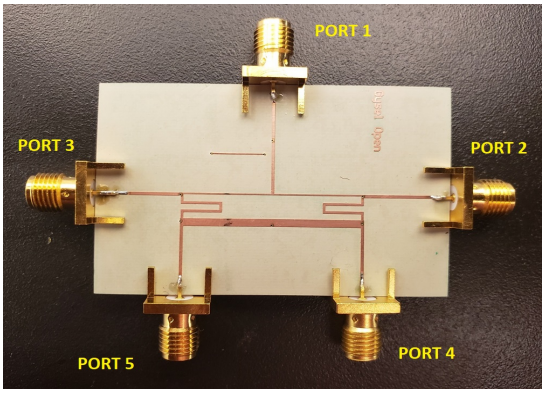

(a) Folded Gysel Combiner Layout(Normal)

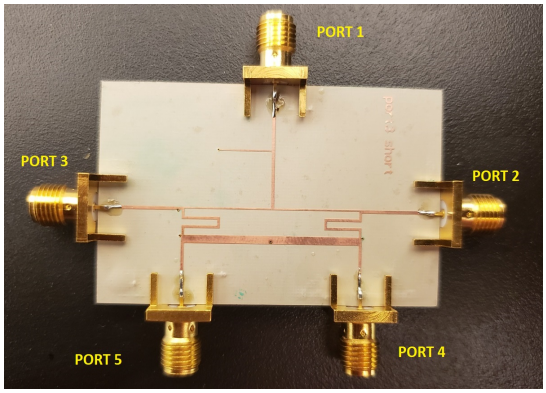

(b) Folded Gysel Combiner Layout(Port3 short)

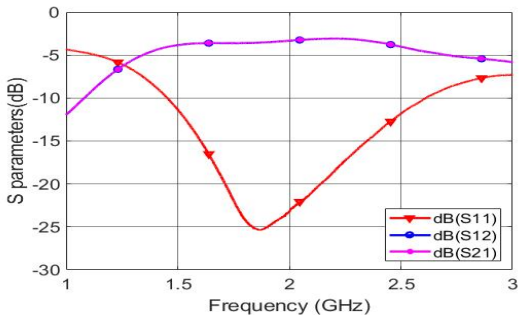

(c) Normal state

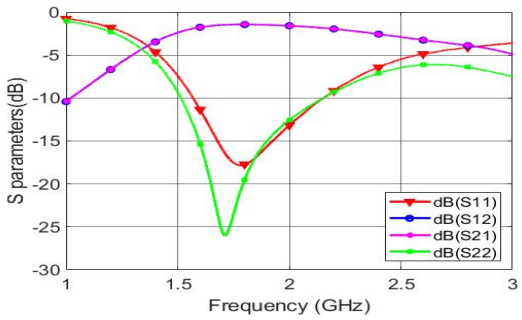

(d) Switch ON state

Figure 3.12: Fabricated layout of folded microstrip GPC and the measurement results for normal and faulty states

Chapter 4

Miniature UWB and Dual-band Filter

Microwave filters are key components in wireless and satellite communication systems. Among which Ultra Wide Band (UWB) and dual-band microstrip filters find use in a wide range of applications. This chapter introduces a unique method to design a UWB and a dual band microstrip filters using a capacitively- coupled distributed microstrip filter integrated with lumped capacitors. For a microstrip filter with N-resonators, the use of the lumped capacitors effectively increases the number of resonators to 2N+1 leading to a significant reduction in the filter size. The chapter also discusses how to use the Ness group delay method [1] to establish an accurate mapping between the ADS circuit model and the Sonnet EM model.

4.1 Narrow-band Five Pole Filter

Consider the 5-pole capacitively-coupled microstrip filter shown in Figure 4.1. It consists of five resonators coupled to each other using capacitive discontinuities. Each of these discontinuities can be represented by a series capacitor in conjunction with two parallel capacitors, as shown in Figure 4.2b. The filter can be designed using the J admittance model following the method presented in[1]. The low-pass g parameter values for the five-pole filter with 0.0138 passband ripple, as listed in Table 4.1.

Figure 4.1: Layout of the narrow band 5 pole filter

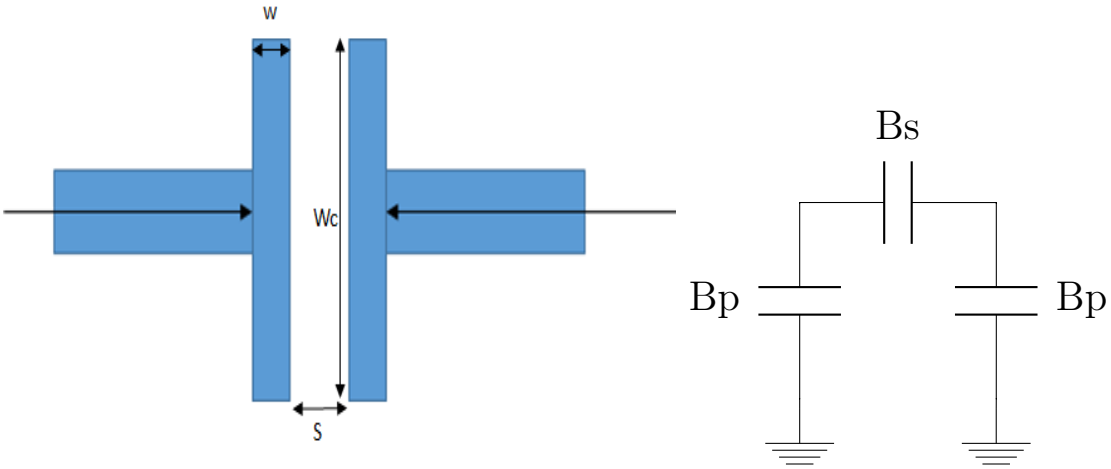

(a) Discontinuity (b) Equivalent model

Figure 4.2: An individual a)capacitive discontinuity and the corresponding b)equivalent circuit model

The required J values are calculated using the low pass g parameters and the fractional bandwidth Δ, as shown below[31].

$$J_{01} = J_{56} = Y_0\sqrt{\Delta\pi/(2g_0g_1)} = 0.0049$$
$$J_{12} = J_{45} = Y_0\Delta\pi/\sqrt{(2g_1g_2)} = 9.4804e^{-}04$$
$$J_{23} = J_{34} = Y_0\Delta\pi/\sqrt{(2g_2g_3} = 6.6453e^{-}04$$

The filter is realized on a substrate with a height of 20 mils and a dielectric constant of 10. Keysight ADS circuit simulator is used to create the S parameters of the capacitive discontinuity model. The gap between the discontinuity (S) is taken as a variable while the other dimensions of the discontinuity are kept constant at Wc=7mm and w=0.1mm. A

Table 4.1: Low pass g parameters[1]

g0	g1	g2	g3	g4	g5	g6
1	0.7965	1.3249	1.6211	1.3249	0.7965	1

lookup table is then created, establishing the relationship between gap S and J admittance values. From the lookup table, the values of S that provide the required J parameter are identified by using the interpolation technique. The gap(S) values corresponding to required J values are S1=S6=0.09mm for J_{01}, S2=S5=0.6mm for J_{12} and S3=S4=0.72mm for J_{23}. Next, the length of the resonator is calculated by adding the corresponding ϕ values. The length of resonators is calculated as TL1=TL5=10.76, TL2=TL4=11.12mm, TL5=11.12mm. A five-pole filter is created using the above dimensions in both ADS circuit model and Sonnet EM model (Figure 4.3a, 4.3b) and the simulation results are shown in Figure 4.3c, 4.3d.

Table 4.2: Lookup table for narrow band filter

S(mm)	S11	S12	J	ϕ
0.08	0.1590 - 0.8890i	0.4220 + 0.0750i	0.0045	-1.394
0.09	0.1710 - 0.8960i	0.4020 + 0.0770i	0.0043	-1.3821
0.1	0.1820 - 0.9020i	0.3840 + 0.0770i	0.0041	-1.3719
0.2	0.2440 - 0.9330i	0.2570 + 0.0670i	0.0027	-1.3151
0.3	0.2690 - 0.9442i	0.1820 + 0.0520i	0.0019	-1.293
0.4	0.2820 - 0.9500i	0.1330 + 0.0390i	0.0014	-1.2823
0.5	0.2880 - 0.9520i	0.0980 + 0.0300i	0.001	-1.277
0.6	0.2910 - 0.9540i	0.0730 + 0.0220i	7.63E-04	-1.2747
0.7	0.2930 - 0.9540i	0.0550 + 0.0170i	5.76E-04	-1.2728
0.8	0.2940 - 0.9550i	0.0420 + 0.0130i	4.40E-04	-1.2721

4.2 Wideband and Dual-band Filter Design

The narrow band filter designed in the previous section can be turned into a wide band or a dual band filter by adding additional lumped capacitors to the capacitive discontinuity, as shown in Figure 4.4. Each capacitive discontinuity together with the lumped capacitor acts as an individual resonator that is coupled to a distributed transmission line resonator.

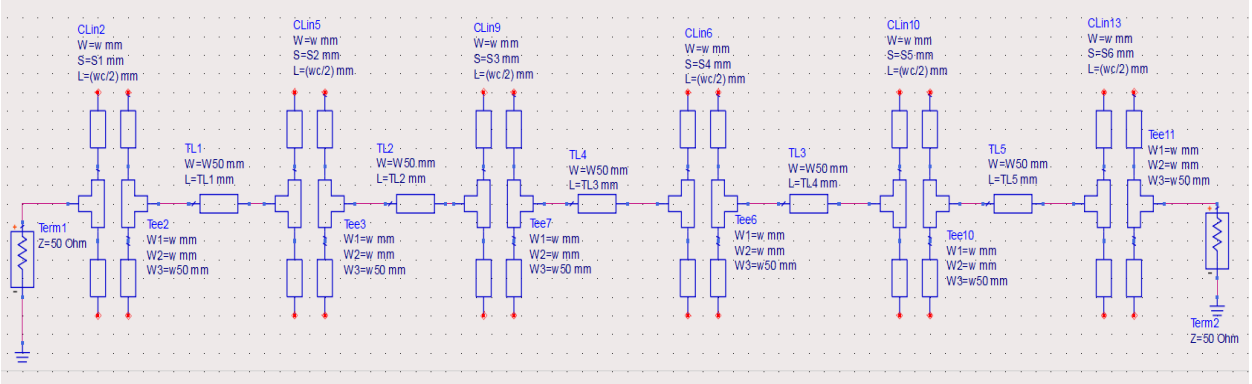

(a) ADS schematic layout

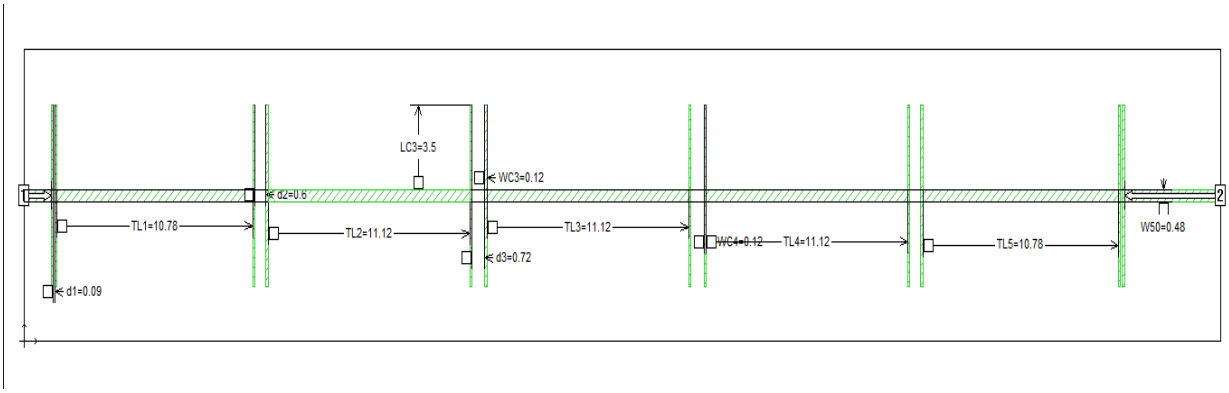

(b) Sonnet layout

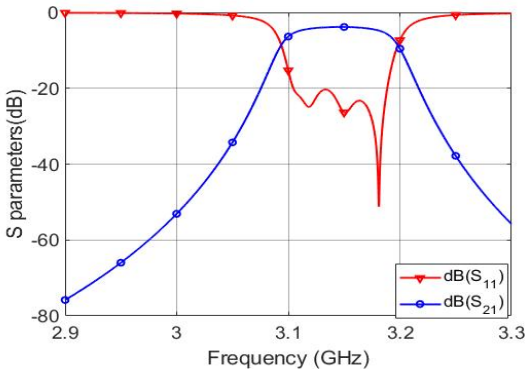

(c) ADS filter response

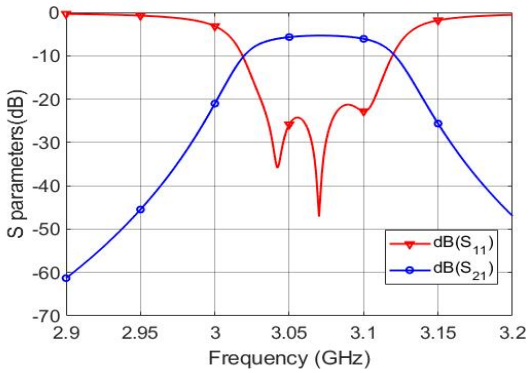

(d) Sonnet filter response

Figure 4.3: Filter design: the narrow band five pole filter layouts from a)ADS, b)Sonnet and response obtained from simulations

Hence, instead of having five resonators, we effectively end up with eleven resonators. By controlling the values of the lumped capacitance we get two sets of resonators. The first set consists of 5 resonators that is formed by the 5 distributed transmission line resonators , while the second set is formed by the capacitive discontinuities/lumped capacitors. Having eleven resonators makes it possible to realize a UWB filter of order 11 if the resonators of the two sets have almost the same resonance frequency. Alternatively, having each set resonating at a particular frequency enable the realization of a dual-band filer. One band with order 5 and the other band is of order 6.

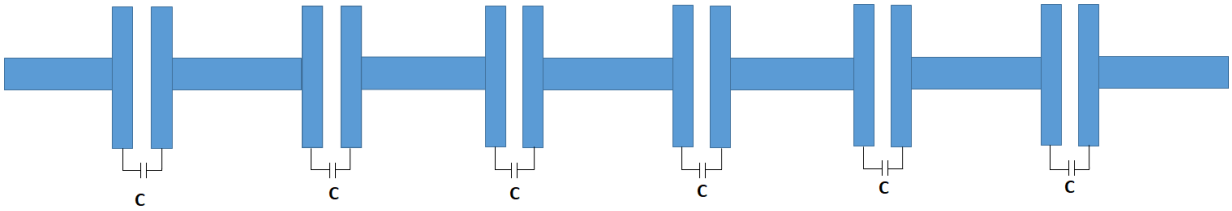

Figure 4.4: A 5 pole filter with the discontinuities attached to lumped capacitors

Let us start by analyzing a single resonator module with one transmission line and two capacitive discontinuities, as shown in Figure 4.5a. The input group delay of the first resonator of the 5-pole microstrip filter is shown in Figure 4.5b. The group delay response shows a single peak. Adding a lumped capacitance C1 to first discontinuity, as shown in Figure 4.5c changes the group delay indicating the presence of two resonance frequencies. The additional peak in the group delay shows the presence of a second resonator corresponding to the capacitive discontinuity/lumped capacitor. Figure 4.5d shows the change that occurs to group delay when the capacitance value C1 varies from 0 to 3pF. When the value of the capacitor is increased, the resonance frequency associated with the capacitive discontinuity shifts down in frequency. The addition of a lumped capacitor C2 to the second capacitive discontinuity creates three resonance frequencies as shown in Figure 4.5e. By controlling the value of C1, C2, the resonant frequencies associated with capacitive discontinuities can be varied.

This proves that adding lumped-element capacitor to the capacitive discontinuities introduces additional resonant frequencies increasing the number of resonators from 5 to 11 without increasing the size of the circuit.

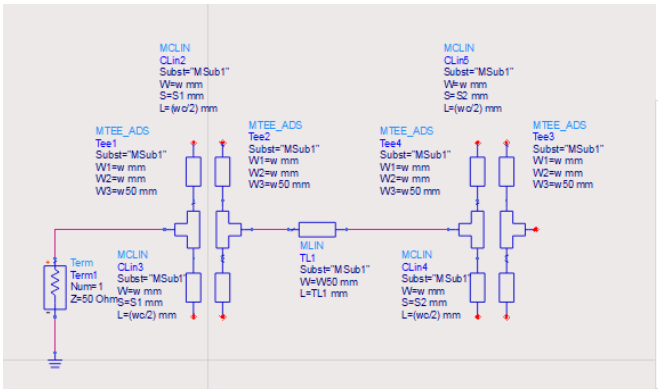

(a) Single resonator module

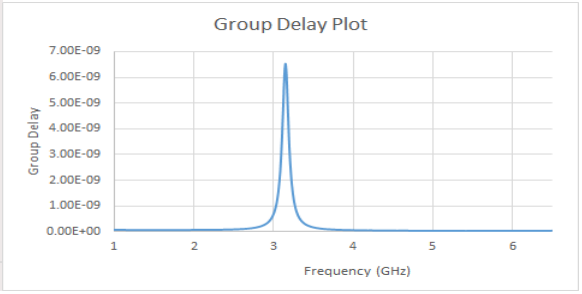

(b) Response

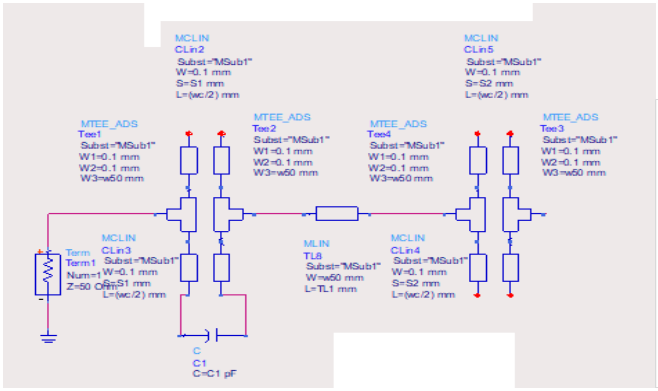

(c) Resonator module with C1

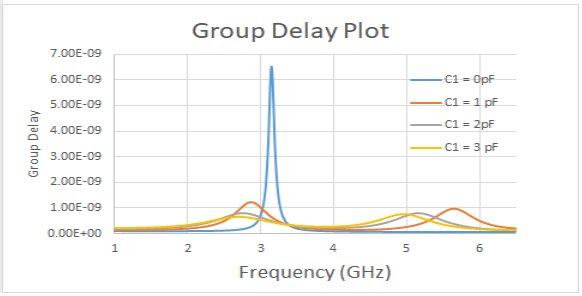

(d) Response

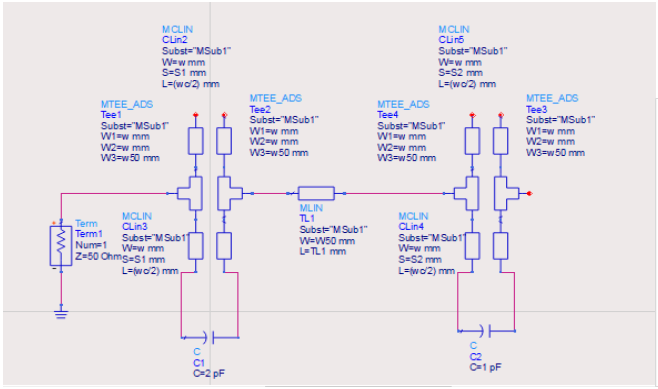

(e) Resonator module with C2

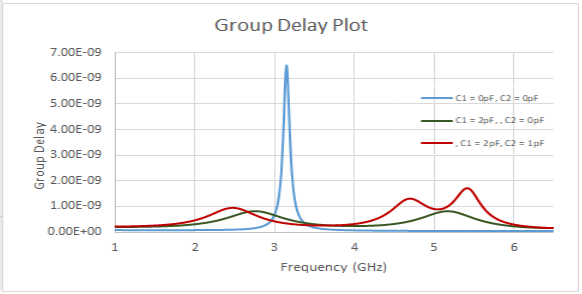

(f) Response

Figure 4.5: The ADS layouts of a single resonator module with and without lumped capacitors and the corresponding group delay plots

4.2.1 Wideband Filter

Figure 4.6a shows the coupling configuration for the wideband filter. The set of 6 resonators that are formed by the capacitive discontinuities and the lumped element capacitors are denoted by "D" and the set of 5 resonators that are formed by the distributed transmission line resonators are denoted by "TL". With the proper choice of circuit dimensions and the lumped element capacitors it is feasible to get the two sets of resonators to have almost the same the resonance frequency to realize an 11-pole filter. Since the adjacent resonators are connected to each other through tapping, large coupling values can be obtained making it feasible to realize an 11-pole UWB filter.

The ADS circuit schematic used for the UWB filter design is shown in Figure 4.6b. Other filter parameters such as Width of discontinuity WC, a gap of discontinuity, Length of transmission line are also used as optimization variables together with the capacitor values. The final wide band filter response after optimization is shown in Figure 4.6c, and the new circuit parameters are listed in Table 4.3.

The ADS schematic parameter values obtained after optimization do not produce the same results in Sonnet EM simulation. Hence Aggressive Space mapping technique is used to create a mapping between ADS schematic and Sonnet. After several optimizations using ASM, the Sonnet EM results are shown in Figure 4.6d, and the new circuit parameters are mentioned in Table 4.3.

Table 4.3: Comparison of parameters of wideband filter from ADS and Sonnet

Parameter	ADS	Sonnet	Parameter	ADS	Sonnet
W50 (Width of Transmission line)	0.47mm	0.47mm	S5 (gap of 5^{th} discontinuity)	0.82mm	0.8mm
TL1 (length of resonator 1)	10.76mm	10.6mm	S6 (gap of 6^{th} discontinuity)	0.28mm	0.3mm
TL2 (length of resonator 2)	11.12mm	10.96mm	WC (Width of discontinuity)	2.48mm	2.3mm
TL3 (length of resonator 3)	11.12mm	11.00mm	C1(Cap of 1^{st} discontinuity)	4pF	4pF
TL4 (length of resonator 4)	11.12mm	10.96mm	C2(Cap of 2^{nd} discontinuity)	2.5pF	2.5pF
TL5 (length of resonator 5)	10.76mm	10.6mm	C3 (Cap of 3^{rd} discontinuity)	2pF	2pF
S1 (gap of 1^{st} discontinuity)	0.3mm	0.3mm	C4 (Cap of 4^{th} discontinuity)	2pF	2pF
S2 (gap of 2^{nd} discontinuity)	0.68mm	0.88mm	C5 (Cap of 5^{th} discontinuity)	2.5pF	2.5pF
S3 (gap of 3^{rd} discontinuity)	1.378mm	1.2mm	C6 (Cap of 6^{th} discontinuity)	4pF	4pF
S4 (gap of 4^{th} discontinuity)	1.387mm	1.5mm	-	-	-

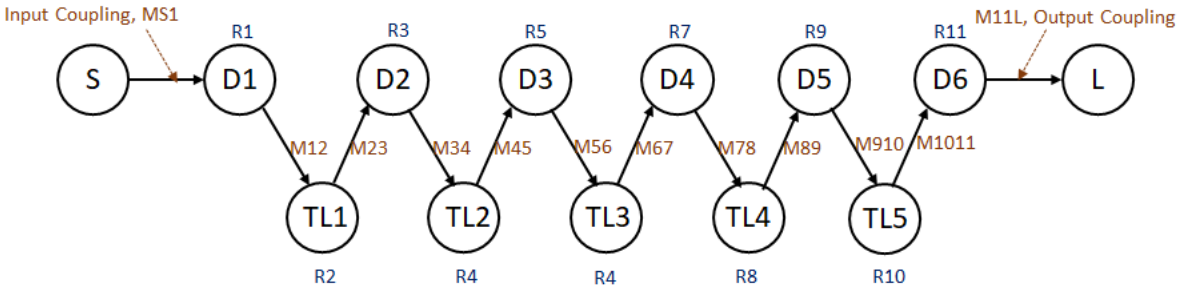

(a) Block diagram showing coupling flow of wideband filter where TL:Transmission line, D:Discontinuity, S:Source, L:Load

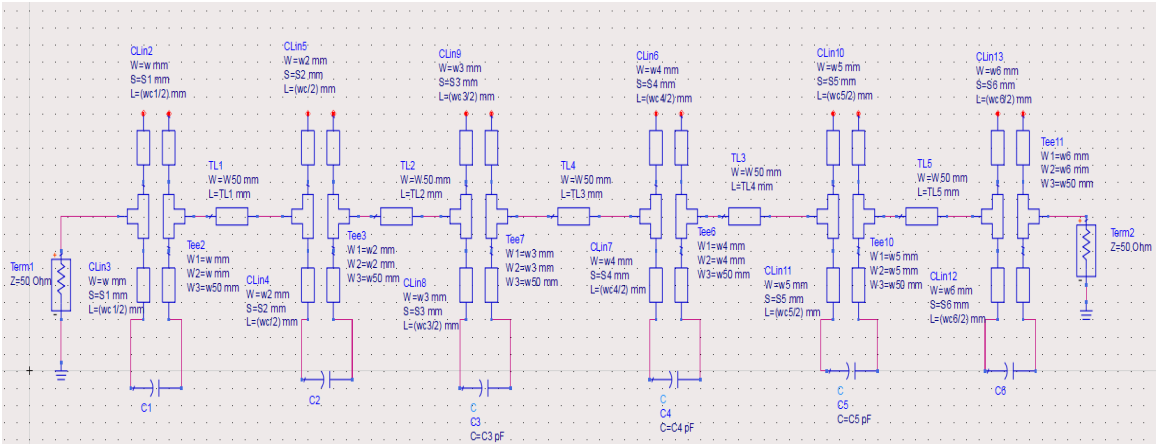

(b) ADS schematic layout

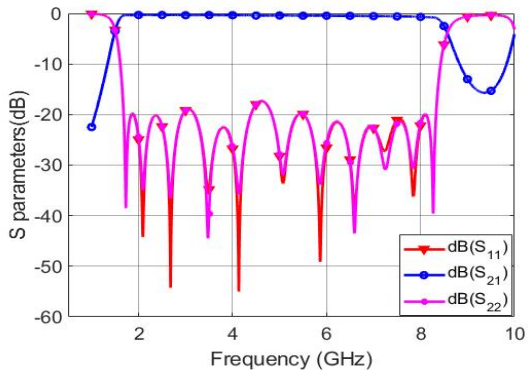

(c) Wideband Filter results from ADS

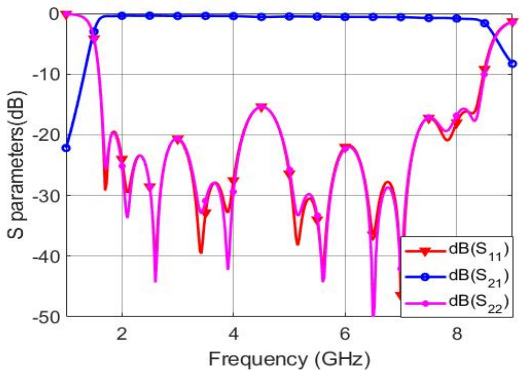

(d) Wideband filter results from Sonnet

Figure 4.6: A block diagram showing the coupling between resonators for a wideband filter incorporated with lumped capacitors, b)the ADS Schematic layout for the wideband filter and the results obtained from c)ADS and d)Sonnet simulations

4.2.2 Dual-band Filter

Figure 4.7a shows the coupling configuration for the dual-band filters. The five resonators of set 1 resonate at frequency f1, while the resonators of set 2 are designed to resonate at frequency f2. The structure can be configured as a dual band filter where for band 1, the resonators of set 2 act as intra-resonator couplings for the resonators in set 1. On the other hand, for band 2, the resonators of band 1 acts as intra-resonator couplings to the resonators of set 1.

The filter parameters such as Width of discontinuity WC, gap of discontinuity (S), Length of transmission line along with capacitor values are optimized using ADS to get a filter with two pass bands (2.1 GHz-3.2 GHz) and (4.7 GHz -6.2 GHz) as shown in Figure 4.7c. Table 4.4 shows the comparison of ADS circuit parameters for narrow band, wide band and dual band circuit.

Table 4.4: Comparison of filter parameters for narroband, UWB and dual-band filter

Parameter	5 pole filter	Wide Band	Dual Band
W50 (Width of Transmission line)	0.47mm	0.47mm	0.47mm
L1 (length of resonator)	10.76mm	9.269mm	10.405mm
TL2 (length of resonator)	11.12mm	9.365mm	10.889mm
TL3 (length of resonator)	11.12mm	9.367mm	11.034m
TL4 (length of resonator)	11.12mm	9.249mm	10.867mm
TL5 (length of resonator)	10.76mm	9.362mm	10.167mm
S1 (gap of first discontinuity)	0.09mm	0.3mm	0.123mm
S2 (gap of second discontinuity)	0.6mm	0.68mm	0.693mm
S3 (gap of third discontinuity)	0.72mm	1.372mm	1.052mm
S4 (gap of fourth discontinuity)	0.72mm	1.387mm	1.077mm
S5 (gap of fifth discontinuity)	0.6mm	0.815mm	0.675mm
S6 (gap of sixth discontinuity)	0.09mm	0.277mm	0.103mm
WC (Width of discontinuity)	7mm	2.48mm	4.48mm
C1 (Cap of first discontinuity)	0pF	4pF	1.7pF
C2 (Cap of second discontinuity)	0pF	2.5pF	0.65pF
C3 (Cap of third discontinuity))	0pF	2pF	0.6pF
C4 (Cap of fourth discontinuity)	0pF	2pF	0.5pF
C5 (Cap of fifth discontinuity))	0pF	2.5pF	0.7pF
C6 (Cap of sixth discontinuity)	0pF	4pF	2pF

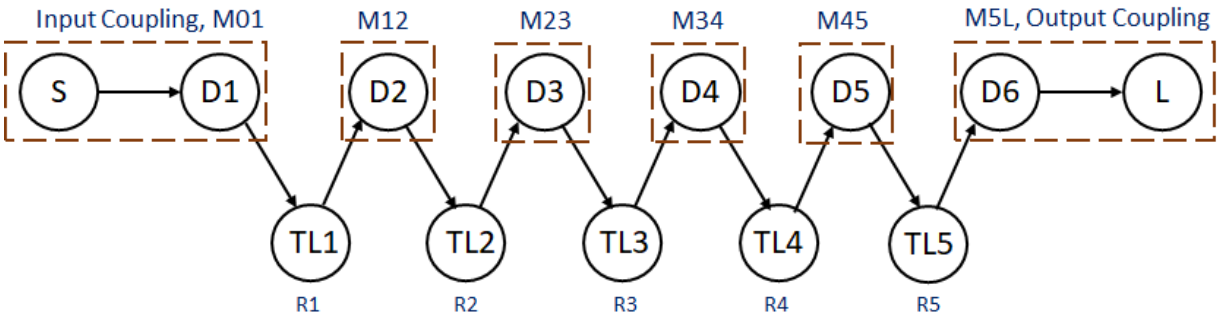

(a) Dual-band filter coupling flow for the first band where TL:Transmission line, D:Discontinuity, S:Source, L:Load

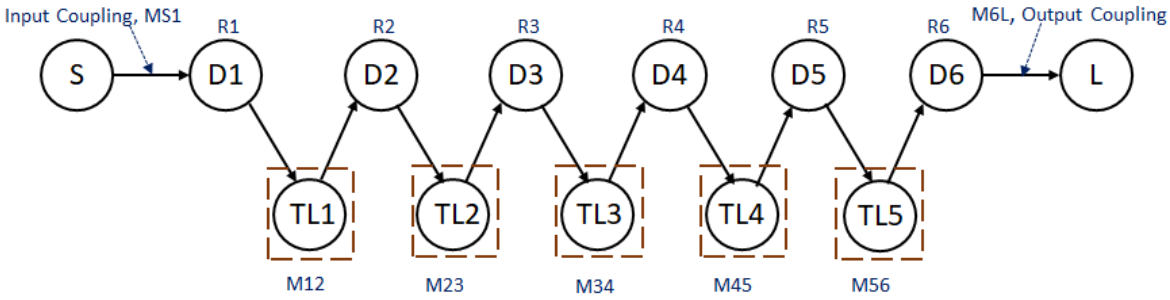

(b) Dual-band filter coupling flow for the second band

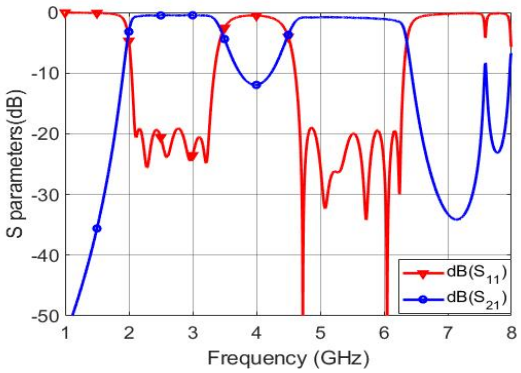

(c) Dual-band filter results from ADS

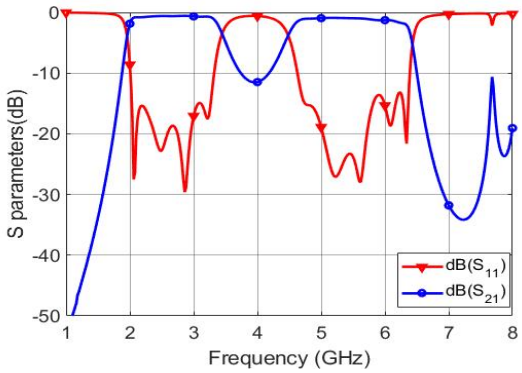

(d) Dual-band filter results from Sonnet

Figure 4.7: The block diagram showing the flow of coupling for dual-band filter for a)first, b)second frequency bands and the results obtained from c) ADS and d)Sonnet simulations

It is evident from Table 4.4 that both wide band and dual band parameters show significant variation from the initial narrow band design. This can be attributed to the adjustments required to compensate for the additional coupling introduced by the lumped capacitors. The dual band design requires lower values for lumped capacitors compared to the wideband, and hence the parameter values of the dual band are closer to the initial 5-pole design. Using the ADS optimized performance as an initial solution, the NESS method is employed to map the EM Sonnet results to the ADS circuit model. The results obtained from Sonnet EM simulation after optimization are shown in Figure 4.7d. The optimization using the Ness method is discussed in the next section.

4.3 Optimization Using Ness Method

In order to use ASM optimization, it is necessary to establish a proper mapping between the ADS course model and the Sonnet EM fine model. However, when the number of optimization parameters is large and the initial results are poor as in the case of a dual band filter, solutions may not converge. Hence for creating the mapping between course model (ADS) and EM fine model(Sonnet) the Ness method [32] using group delay optimization technique is utilised. The following section explains how we used the Ness method for optimization and effectively transferring the dual band filter ADS schematic design into the Sonnet EM design.

Figure 4.8a shows the ADS schematic of a three-pole dual band filter with lumped capacitors designed using the previous technique and Figure 4.8b shows the filter response. The group delay of the input reflection coefficient (S11) has sufficient information and can be used to design any filter. So, the next objective is to transfer the design into Sonnet using Ness method group delay optimization. The steps involved in the design are described below.

In the ADS schematic, detune all resonators except the first one (first discontinuity), and use the same dimensions in Sonnet and find the group delay response. The leading figure in Figure 4.9 shows the group delay from ADS and Sonnet for the same dimensions. The Sonnet EM response shows a significant variation from the ADS schematic results; hence, optimization is required to achieve the same value for the group delay. In this case, there are three optimization variables Width of discontinuity (WC1), Gap of discontinuity (S1) and Length of discontinuity (W1). It is optimized until the EM group delay is the same as the ADS group delay as shown in Figure 4.9(2) and the new dimensions are listed in Table 4.5.

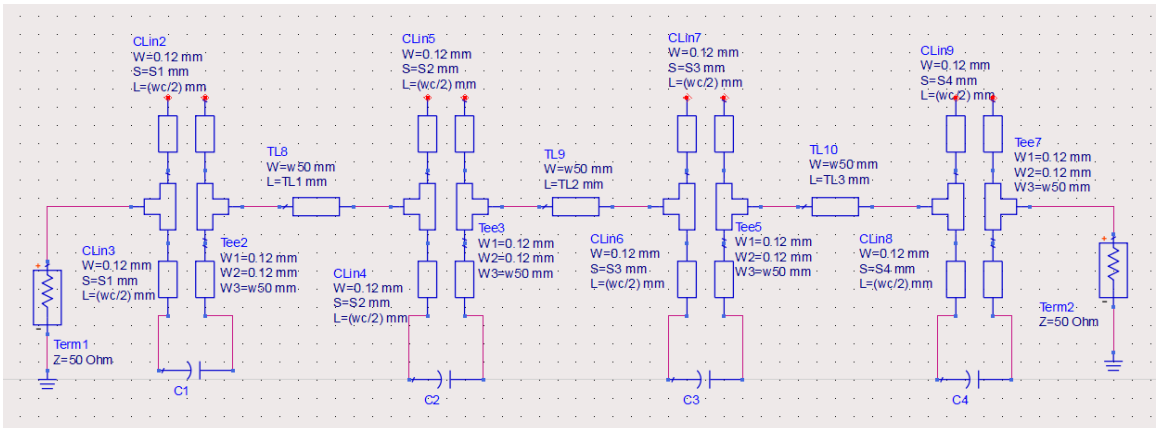

(a) ADS schematic of a 7pole filter

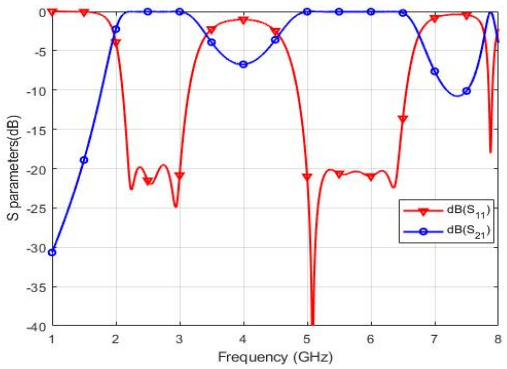

(b) ADS dual-band filter response

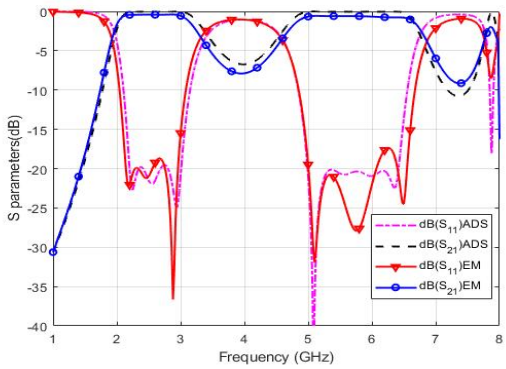

(c) Sonnet dual-band filter response

Figure 4.8: The ADS schematic layout of 7 pole dual-band filter used for the design, initial results from ADS and the final results from Sonnet after optimization

In the next step, all resonators except resonators 1, 2 are detuned, and the variables are adjusted using Sonnet to reproduce the same group delay response as shown in Figure 4.9(3). Similarly each resonator is added sequentially until the last one and the parameters are optimized to replicate the group delay response of the ADS circuit schematic. The filter design is completed after the group delay is sequentially matched with the ideal circuit response. The dimensions after the addition of each step is listed in Table 4.5 and the final EM filter response is shown in Figure 4.8c.

Figure 4.9: The results obtained from group delay optimization using Ness method after incorporating each resonators

Table 4.5: Parameter values obtained from group delay optimization

Parameter	opt1	opt2	opt3	opt4	opt5	opt6	opt7	ADS
W1	0.22mm	0.22mm	0.22mm	0.22mm	0.22mm	0.22mm	0.22mm	0.16mm
WC1	1.96mm	1.96mm	1.96mm	1.96mm	1.96mm	1.96mm	1.96mm	2.24mm
S1	0.12mm	0.12mm	0.12mm	0.12mm	0.12mm	0.12mm	0.12mm	0.18mm
TL1	-	10.26mm	10.26mm	10.26mm	10.26mm	10.26mm	10.26mm	10.43mm
W2	-	-	0.22mm	0.22mm	0.22mm	0.22mm	0.22mm	0.22mm
WC2	-	-	2mm	2mm	2mm	2mm	2mm	2.24mm
S2	-	-	1.1mm	1.1mm	1.1mm	1.1mm	1.1mm	1.09mm
TL2	-	-	-	11.06mm	11.06mm	11.06mm	11.06mm	11.251mm
W3	-	-	-	-	0.22mm	0.22mm	0.22mm	0.16mm
WC3	-	-	-	-	2mm	2mm	2mm	2.24mm
S3	-	-	-	-	1.4mm	1.4mm	1.4mm	1.408mm
TL3	-	-	-	-	-	10.42mm	10.42mm	10.623mm
W4	-	-	-	-	-	-	0.22mm	0.16mm
WC4	-	-	-	-	-	-	1.94mm	2.24mm
S4	-	-	-	-	-	-	0.5mm	0.5mm

4.4 Wideband and Dual-band Filter Design for Lower Frequency

The filters discussed in the previous sections are designed for the higher frequency range 2-8.5GHz. It is interesting to see a filter designed for the lower frequency range with the same technique. This also makes it easy to use lumped-element capacitors with a reasonably low self-resonance frequency. Starting with a 5-pole narrow band filter designed at a lower frequency can reduce the design time. Hence the first step is to design a narrow band filter for the lower frequency (1.5GHz) as shown in Figure 4.10a. This is a good starting point for the wide band and dual band filter design. The dimensions for the narrow band filter are listed in Table 4.6.

The steps followed in the previous sections are repeated and a wide band filter ranging from 1.8GHz to 3.7GHz is obtained as shown in Figure 4.10b. A low frequency dual-band filter was also designed. Figure 4.10c illustrates the results obtained from the design. A comparison of parameter values obtained from the three designs are listed in Table 4.6.

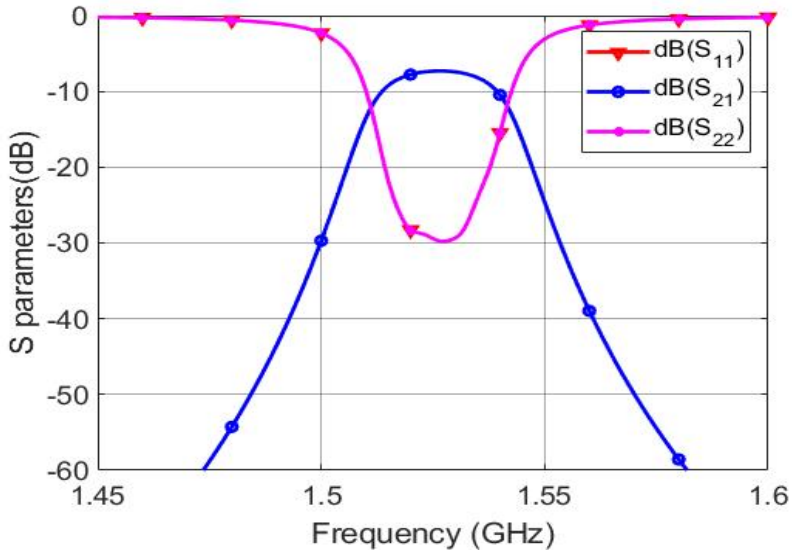

(a) Narrow band filter Layout

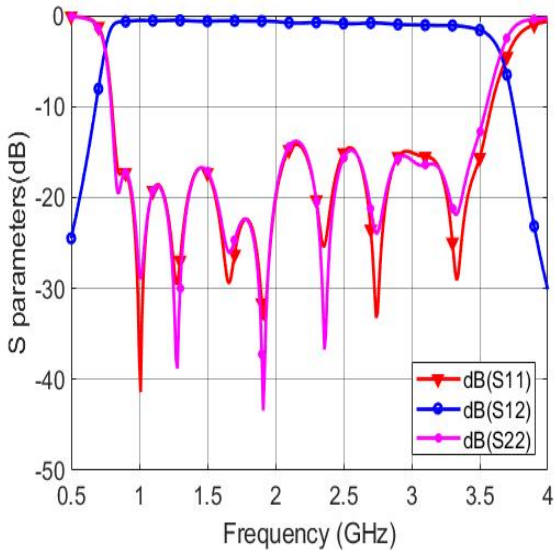

(b) Wideband filter

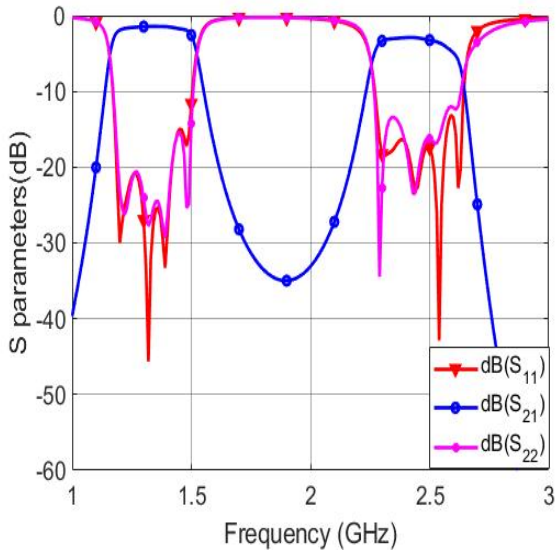

(c) Dual-band Filter

Figure 4.10: The results obtained from Sonnet simulation for low frequency design of a)narrow band,b)wide band and a)dual-band filter

Table 4.6: Comparison of filter parameters for lower frequency design

Parameter	5 pole filter	Wide Band	Dual Band
W50 (Width of Transmission line)	0.47mm	0.47mm	0.47mm
TL1 (length of resonator)	27.97mm	16.639mm	16.268mm
TL2 (length of resonator)	31.13mm	15.447mm	17.917mm
TL3 (length of resonator)	31.14mm	16.704mm	18.282m
TL4 (length of resonator)	31.13mm	16.178mm	18.099mm
TL5 (length of resonator)	27.97mm	18.224mm	16.614mm
S1 (gap of first discontinuity)	0.1mm	1.899mm	0.209mm
S2 (gap of second discontinuity)	0.615mm	0.646mm	0.615mm
S3 (gap of third discontinuity)	0.76mm	1.9mm	1.042mm
S4 (gap of fourth discontinuity)	0.76mm	1.94mm	0.974mm
S5 (gap of fifth discontinuity)	0.615mm	0.46mm	0.534mm
S6 (gap of sixth discontinuity)	0.1mm	2mm	0.113mm
WC1 (Width of discontinuity 1)	6mm	6.21mm	16.112mm
WC2 (Width of discontinuity 2)	6mm	8.87mm	17.37mm
WC3 (Width of discontinuity 3)	6mm	8.762mm	17.126mm
WC4 (Width of discontinuity 4)	6mm	8.984mm	17.126mm
WC5 (Width of discontinuity 5)	6mm	9.271mm	17.37mm
WC6 (Width of discontinuity 6)	6mm	7.285mm	16.112mm
C1 (Cap of first discontinuity)	0pF	6.5pF	2.4pF
C2 (Cap of second discontinuity)	0pF	5.3pF	0.8pF
C3 (Cap of third discontinuity))	0pF	3.8pF	0.65pF
C4 (Cap of fourth discontinuity)	0pF	3.8pF	0.65pF
C5 (Cap of fifth discontinuity))	0pF	5.3pF	0.6pF
C6 (Cap of sixth discontinuity)	0pF	6.3pF	3pF

4.5 Experimental Results

Figure 4.11 shows the layout and experimental results obtained for the wideband and dual-band filters.

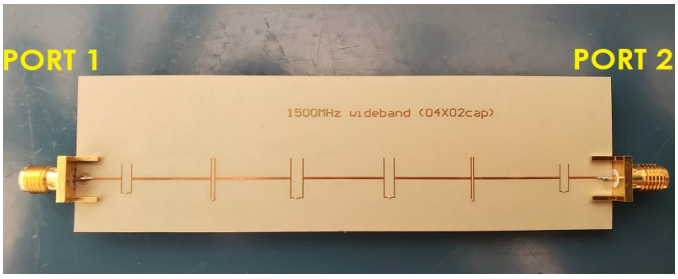

(a) Wideband filter layout

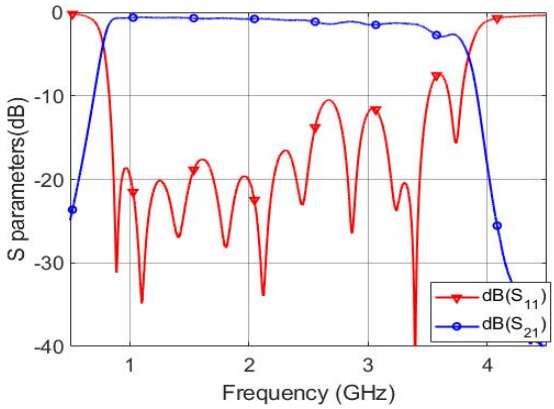

(b) Wideband filter

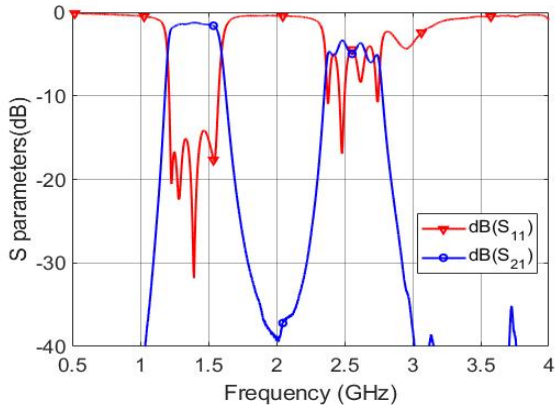

(c) Dual-band Filter

Figure 4.11: The measured results obtained from b)wide band and a)dual-band filter

Chapter 5

Conclusion

This thesis introduced unique designs for a reconfigurable Gysel Power Combiner and miniature filter design that can operate as UWB filter or dual-band filter. An extensive overview of the Gysel power combiner and work done by various researchers in the past has been described in Chapter 2. A reconfigurable Gysel combiner incorporating switches and a matching network has been presented in Chapter 3. It allows the combiner to work efficiently in normal operation or in the case of failure of one of the amplifiers.

A highly miniature filter has been proposed in Chapter 4. The proposed filter configuration introduces lumped capacitors to a conventional capacitively-coupled microstrip filter with N resonators to increase the number of resonators to 2N+1 resonators. The value of the lumped capacitor determines the new resonating frequencies hence it plays a major role in deciding the behaviour of the filter. These filters can operate as a UWB filter or a dual-band filter based on the capacitance values.

Simulation and measured results have been presented for the Gysel combiner and miniature UWB and dual-band filters. Initial designs are carried out in Keysight ADS schematic software and final circuit designs have been verified using Sonnet EM simulations. The Aggressive space mapping technique and the Ness method are utilized for the accurate mapping between ADS Schematic and Sonnet EM Simulator. The measured results obtained for the prototype units fabricated for the Gysel coupler, UWB and dual-band filter verify the concepts proposed in this thesis.

Future Works

Next target is to design a CPW based reconfigurable Gysel Power Combiner. The 2N+1 resonator dual-band filter designed in the thesis has relatively poor isolation between the two bands. Hence another focus is to improve the isolation between the bands. Also the UWB and dual band filter presented in the thesis have different dimensions. Future works are focused in achieving a filter that can reconfigured as a UWB filter or a dual band filter using varactors.

.

References

[1] J. Cameron Richard, R. Mansour Raafat, and M. Kudsia Chandra. *Microwave Filters for Communication Systems: Fundamentals, Design, and Applications*. 2nd edition edition.

[2] Zhang Haiwei and Xue Quan. A novel Gysel power divider with arbitrary power ratio for high-power application. In *2013 IEEE International Wireless Symposium (IWS)*, pages 1–4, April 2013.

[3] Jianzhong He, Weikang Luo, and Shiyong Chen. A Gysel power divider with enhanced isolation bandwidth. In *2015 Asia-Pacific Microwave Conference (APMC)*, volume 3, pages 1–3, December 2015.

[4] Jin Guan, Lijun Zhang, Zhengyu Sun, Yongqing Leng, and Yatao Peng. Designing power divider by combining wilkinson and gysel structure. *Electronics Letters*, 48(13):769–770, June 2012.

[5] E.J. Wilkinson. An N-Way Hybrid Power Divider. *IRE Transactions on Microwave Theory and Techniques*, 8(1):116–118, January 1960.

[6] Yongle Wu, Lingxiao Jiao, Zheng Zhuang, and Yuanan Liu. The art of power dividing: A review for state-of-the-art planar power dividers. *China Communications*, 14(5):1–16, May 2017.

[7] U.H. Gysel. A New N-Way Power Divider/Combiner Suitable for High-Power Applications. In *1975 IEEE-MTT-S International Microwave Symposium*, pages 116–118, May 1975.

[8] Yongle Wu, Yuanan Liu, Quan Xue, Shulan Li, and Cuiping Yu. Analytical Design Method of Multiway Dual-Band Planar Power Dividers With Arbitrary Power Division. *IEEE Transactions on Microwave Theory and Techniques*, 58(12):3832–3841, December 2010.

[9] M.-j. Park. Coupled line Gysel power divider for dual-band operation. *Electronics Letters*, 47(10):599 –601, May 2011.

[10] H.W. Zhang, X.W. Shi, Feng Wei, and Le Xu. Compact wideband Gysel power divider with arbitrary power division based on patch type structure. *Progress In Electromagnetics Research*, 119, January 2011.

[11] Hongchang Xiao, Yuan Quan, and Shiyong Chen. Microstrip anti-phase Gysel power divider with unequal power division. In *2017 IEEE 2nd Advanced Information Technology, Electronic and Automation Control Conference (IAEAC)*, pages 846–849, March 2017.

[12] Ban-Leong Ooi, W. Palei, and M.S. Leong. Broad-banding technique for in-phase hybrid ring equal power divider. *IEEE Transactions on Microwave Theory and Techniques*, 50(7):1790–1794, July 2002.

[13] Homayoon Oraizi and Ali-Reza Sharifi. Optimum Design of Asymmetrical Multisection Two-Way Power Dividers With Arbitrary Power Division and Impedance Matching. *IEEE Transactions on Microwave Theory and Techniques*, 59(6):1478–1490, June 2011.

[14] Homayoon Oraizi and Ali-Reza Sharifi. Optimum Design of a Wideband Two-Way Gysel Power Divider With Source to Load Impedance Matching. *IEEE Transactions on Microwave Theory and Techniques*, 57(9):2238–2248, September 2009.

[15] Mohammad A. Maktoomi and Mohammad S. Hashmi Indraprastha. A novel power divider structure using the gysel and wilkinson power dividers with only one grounded resistor. In *2015 IEEE MTT-S International Microwave and RF Conference (IMaRC)*, pages 227–229, December 2015. ISSN: 2377-9152.

[16] Zhengyu Sun, Lijun Zhang, Yuzhe Liu, and Xiaodong Tong. Modified Gysel Power Divider for Dual-Band Applications. *IEEE Microwave and Wireless Components Letters*, 21(1):16–18, January 2011.

[17] Hamed Shahi Gharehaghaji and Hossein Shamsi. Modified dual band gysel power divider with isolation bandwidth improvement. In *2016 24th Iranian Conference on Electrical Engineering (ICEE)*, pages 1801–1804, May 2016. ISSN: null.

[18] Xue Ren, Kaijun Song, Maoyu Fan, Yu Zhu, and Bingkun Hu. Compact Dual-Band Gysel Power Divider Based on Composite Right- and Left-Handed Transmission Lines. *IEEE Microwave and Wireless Components Letters*, 25(2):82–84, February 2015.

[19] Fu-Xing Liu, Yang Wang, Xiao-Yu Zhang, Chun-He Quan, and Jong-Chul Lee. A new multi-band Gysel power divider. In *2018 IEEE MTT-S International Wireless Symposium (IWS)*, pages 1–4, May 2018.

[20] Shiyong Chen, Yantao Yu, and Mingchun Tang. Dual-Band Gysel Power Divider With Different Power Dividing Ratios. *IEEE Microwave and Wireless Components Letters*, 29(7):462–464, July 2019.

[21] Z. Sun, L. Zhang, and Y. Yan. A novel unequal dual-band Gysel power divider. In *2011 IEEE MTT-S International Microwave Symposium*, pages 1–1, June 2011. ISSN: 0149-645X, 0149-645X, 0149-645X.

[22] Lingxiao Jiao, Yongle Wu, and Yuanan Liu. A novel impedance-transforming coupled-line power divider combining Wilkinson and Gysel structures. In *2016 IEEE International Workshop on Electromagnetics: Applications and Student Innovation Competition (iWEM)*, pages 1–3, May 2016. ISSN: null.

[23] Xi Wang, Ke-Li Wu, and Wen-Yan Yin. A Compact Gysel Power Divider With Unequal Power-Dividing Ratio Using One Resistor. *IEEE Transactions on Microwave Theory and Techniques*, 62(7):1480–1486, July 2014.

[24] Feng Lin, Qing-Xin Chu, Zhi Gong, and Zhe Lin. Compact Broadband Gysel Power Divider With Arbitrary Power-Dividing Ratio Using Microstrip/Slotline Phase Inverter. *IEEE Transactions on Microwave Theory and Techniques*, 60(5):1226–1234, May 2012.

[25] D. Deslandes and K. Wu. Integrated microstrip and rectangular waveguide in planar form. *IEEE Microwave and Wireless Components Letters*, 11(2):68–70, February 2001.

[26] Orcun Kiris, Volkan Akan, Mesut Gokten, and Lokman Kuzu. Three-way substrate integrated waveguide (SIW) power divider design. In *2016 IEEE/ACES International Conference on Wireless Information Technology and Systems (ICWITS) and Applied Computational Electromagnetics (ACES)*, pages 1–2, March 2016. ISSN: null.

[27] Haidong Chen, XiaoQing Wang, Wenquan Che, YiHua Zhou, and Tingting Liu. Novel Gysel power dividers based on Half-Mode Substrate Integrated Waveguide (HMSIW). In *2018 IEEE MTT-S International Wireless Symposium (IWS)*, pages 1–3, May 2018. ISSN: null.

[28] Haidong Chen, Wenquan Che, Xiaoqing Wang, and Wenjie Feng. Size-Reduced Planar and Nonplanar SIW Gysel Power Divider Based on Low Temperature Co-fired Ceramic

Technology. *IEEE Microwave and Wireless Components Letters*, 27(12):1065–1067, December 2017.

[29] Wei Hong, Bing Liu, Yuanqing Wang, Qinghua Lai, Hongjun Tang, Xiao Xin Yin, Yuan Dan Dong, Yan Zhang, and Ke Wu. Half Mode Substrate Integrated Waveguide: A New Guided Wave Structure for Microwave and Millimeter Wave Application. In *2006 Joint 31st International Conference on Infrared Millimeter Waves and 14th International Conference on Teraherz Electronics*, pages 219–219, September 2006. ISSN: 2162-2035.

[30] J.W. Bandler, R.M. Biernacki, Shao Hua Chen, R.H. Hemmers, and K. Madsen. Electromagnetic optimization exploiting aggressive space mapping. *IEEE Transactions on Microwave Theory and Techniques*, 43(12):2874–2882, December 1995.

[31] David M. Pozar. *Microwave Engineering, 4th edition.*

[32] J.B. Ness. A unified approach to the design, measurement, and tuning of coupled-resonator filters. *IEEE Transactions on Microwave Theory and Techniques*, 46(4):343–351, April 1998.